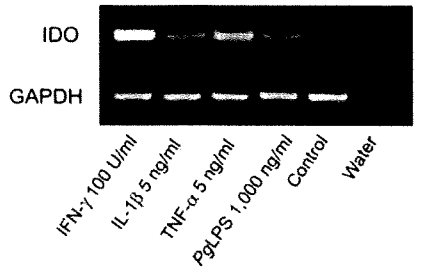

Figure 2.
IDO mRNA expression of HGF cells upon stimualtion with IFN-γ, IL-1β, TNF-α, and PgLPS. Unstimulated HGFs served as a control.

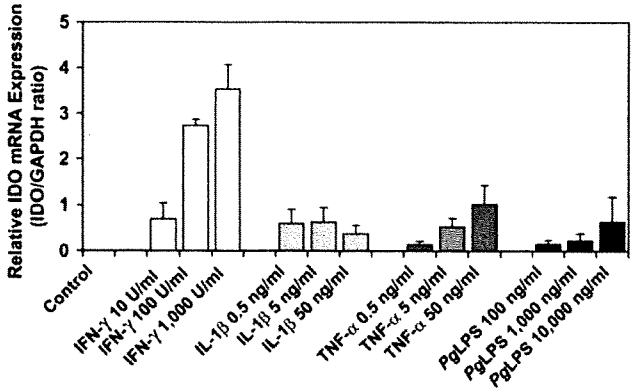

Figure 3.
Relative IDO mRNA expression in HGF cells treated with different concentrations of IFN-γ, IL-1β, TNF-α, or PgLPS. Data are shown as mean ± SE from four separate experiments.

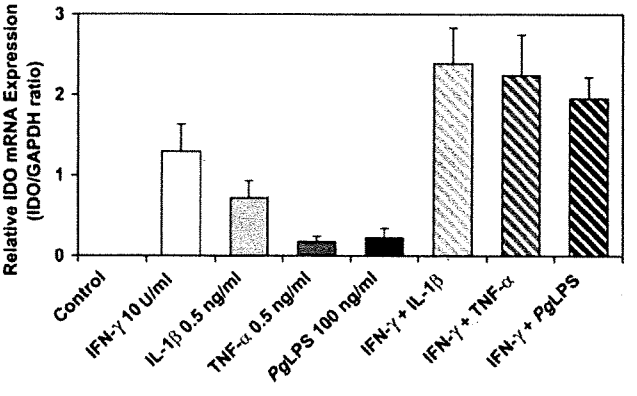

Figure 4.
Relative IDO mRNA expression in HGF cells treated with combinations of IFN-γ and IL-1β, TNF-α, or PgLPS. Data are shown as mean ± SE from four separate experiments.

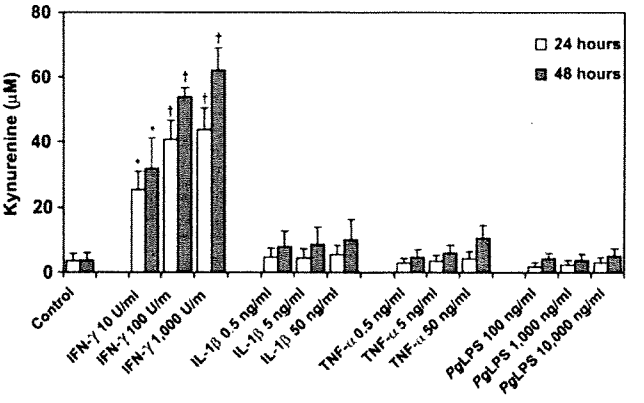

Figure 5.
*IDO activity in HGF cells treated with different concentrations of IFN-γ, IL-1β, TNF-α, or PgLPS. Data are shown as mean ± SE from four separate experiments. Significantly different from the untreated control: *P <0.05; †P <0.01.*

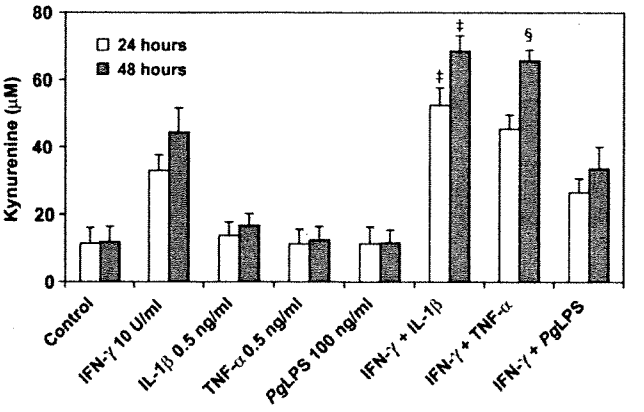

Figure 6.
IDO activity in HGF cells treated with combinations of IFN-γ and IL-1β, TNF-α, or PgLPS. Data are shown as mean ± SE from four separate experiments. Significantly different from IFN-γ alone: ‡P <0.05; §P <0.01.

than in that of healthy gingiva. We observed a strong nuclear staining pattern within epithelial cells. IDO was reported to be an intracellular enzyme. Cytoplasmic staining of IDO was observed in peripheral blood mononuclear cells,[27] stromal cells, luminal and glandular epithelial cells of human placenta,[28] and ovarian cancer cells.[29] However, there was a report[30] of IDO immunostaining localized primarily to the nuclei of placental endothelial cells. How IDO translocates to the nucleus and whether it also has a nuclear function are not known.

In gingival connective tissue, the level and extent of IDO expression were also higher in periodontitis tissues than that of healthy tissues. Periodontitis lesions had high levels of several inflammatory cytokines and bacterial products that were inducers of IDO.[17-19] Therefore, upregulation of IDO expression in periodontitis lesions may be due to the presence of these agents. In this study, we assessed IDO expression of

cultured HGFs upon stimulation with IFN-γ, IL-1β, TNF-α, and *Pg*LPS. Gingival fibroblasts are the major cell type within periodontal tissues and may participate directly with several inflammatory mediators in periodontitis. We found that HGFs did not constitutively express IDO; however, IDO expression was inducible in these cells. IFN-γ is a potent inducer for IDO expression in HGFs. Lower levels of IDO expression were detected upon stimulation with IL-1β, TNF-α, and *Pg*LPS. IFN-γ was shown to be a strong inducer of IDO expression in many cell types, including dendritic cells, macrophages, epithelial cells, skin fibroblasts, and many cancer cell lines.[14,31,32] It was shown that the IDO promoter contains the interferon-stimulated response element (ISRE) and gamma-activated sequence (GAS). These sequences were the binding site for the transcription factor IFN-regulatory factor-1 (IRF-1) and signal transducer and activator of transcription 1 (STAT1), which allowed activation of the IDO gene in response to IFN-γ.[33]

We showed that IL-1β, TNF-α, and *Pg*LPS, when used as a single agent, induced low levels of IDO expression in HGFs. TNF-α alone was ineffective in IDO induction of peripheral blood mononuclear cells, macrophages, epithelial cell line, and an astrocytoma cell line,[5,15,34] but it showed weak IDO induction in a fibroblast cell line.[35] IL-1 alone also was unable to induce IDO expression in macrophages[36] or epithelial cells.[15] Bacterial LPS induced IDO expression in dendritic cells[37] and monocyte-derived macrophages[16] but not in epithelial cells from the cervix[15] or lung.[34] Therefore, IDO expression in response to inflammatory cytokines and mediators seems to be cell-type specific.

IFN-γ in combination with IL-1β, TNF-α, or *Pg*LPS augmented the level of IDO expression in HGFs compared to IFN-γ alone. Combinations of IFN-γ and IL-1β as well as IFN-γ and TNF-α also increased IDO expression in human monocyte–derived macrophages and human cervical epithelial cells.[15,36] The synergistic effect of TNF-α and IFN-γ on IDO induction was shown to be mediated at the level of transcription through an increase in IFN-γ receptor expression that enhanced the binding of STAT1 to GAS and IRF-1 to ISRE sites.[33] The combination effect of inflammatory cytokines and bacterial products on IDO expression may be important for regulating IDO function in vivo.

The control of IDO activity seems to be complex and cell-type specific. The presence of IDO mRNA and protein may not correlate with its functional activity. Human dendritic cells constitutively express IDO protein, but the protein does not have functional enzymatic activity until these cells are activated by IFN-γ and cluster of differentiation (CD) 80/CD86 ligation.[38] In this study, we showed that increased IDO mRNA expression in HGFs upon treatment with IFN-γ was positively correlated with increased IDO activity. In addition, the IDO activity was increased over time. However, IDO activity in HGFs treated with IL-1β, TNF-α, or *Pg*LPS was not significantly different from that of untreated controls. This may be due to the low level of IDO mRNA expression in these cells and the wide variation in the level of response between primary cell lines. We also showed that IL-1β and TNF-α augmented the IDO activity in IFN-γ–treated HGF cells. IL-1β, TNF-α, and LPS were shown to enhance the IDO activity induced by IFN-γ in human monocyte–derived macrophages.[16,36] In contrast, the presence of IL-1β and TNF-α decreased the IDO activity induced by IFN-γ in a uroepithelial cell line and showed no effect on the IDO activity induced by IFN-γ in an astrocytoma cell line.[5] It seemed that HGFs were able to produce functional IDO in response to several inflammatory cytokines and immunomodulating agents. These agents may work together or regulate each other to control IDO expression and activity in periodontal tissues.

The role of IDO in periodontal disease pathogenesis is not known. A previous study[39] from our laboratory showed that coculturing of peripheral blood mononuclear cells with HGF cells treated with IFN-γ and *Pg*LPS resulted in the suppression of T-cell proliferation. This effect could be reversed by the addition of 1-metyl-tryptophan, an inhibitor of IDO. Therefore, IDO expression may be one of several mechanisms to downregulate the inflammatory process in periodontitis. This effect may be beneficial to the host and prevent excessive inflammation and the destruction of periodontal tissues. Further studies are needed to explore this hypothesis.

CONCLUSIONS

IDO was expressed in human gingiva, and the expression was upregulated in chronic periodontitis. The increased IDO expression in periodontitis lesions may be due, in part, to the activation of HGFs by inflammatory cytokines and bacterial products.

ACKNOWLEDGMENTS

This study was supported by grants from the Thailand Research Fund (MRG4980177) and the Ratchadapisek Research Fund, Bangkok, Thailand. The authors thank Dr. Osamu Takikawa for the IDO-specific monoclonal antibody and suggestions on manuscript preparation. We also thank Dr. Robert E. Schifferle, Department of Oral Biology and Periodontology, University at Buffalo, Buffalo, New York, for the *Pg*LPS. The authors report no conflicts of interest related to this study.

REFERENCES

1. Takikawa O. Biochemical and medical aspects of the indoleamine 2,3-dioxygenase-initiated l-tryptophan

metabolism. *Biochem Biophys Res Commun* 2005; 338:12-19.
2. Pfefferkorn ER, Eckel M, Rebhun S. Interferon-gamma suppresses the growth of *Toxoplasma gondii* in human fibroblasts through starvation for tryptophan. *Mol Biochem Parasitol* 1986;20:215-224.
3. Pantoja LG, Miller RD, Ramirez JA, Molestina RE, Summersgill JT. Inhibition of *Chlamydia pneumoniae* replication in human aortic smooth muscle cells by gamma interferon-induced indoleamine 2, 3-dioxygenase activity. *Infect Immun* 2000;68:6478-6481.
4. Hayashi T, Rao SP, Takabayashi K, et al. Enhancement of innate immunity against *Mycobacterium avium* infection by immunostimulatory DNA is mediated by indoleamine 2,3-dioxygenase. *Infect Immun* 2001;69:6156-6164.
5. Daubener W, MacKenzie CR. IFN-gamma activated indoleamine 2,3-dioxygenase activity in human cells is an antiparasitic and an antibacterial effector mechanism. *Adv Exp Med Biol* 1999;467:517-524.
6. Bodaghi B, Goureau O, Zipeto D, Laurent L, Virelizier JL, Michelson S. Role of IFN-gamma-induced indoleamine 2,3 dioxygenase and inducible nitric oxide synthase in the replication of human cytomegalovirus in retinal pigment epithelial cells. *J Immunol* 1999; 162:957-964.
7. Adams O, Besken K, Oberdorfer C, MacKenzie CR, Russing D, Daubener W. Inhibition of human herpes simplex virus type 2 by interferon gamma and tumor necrosis factor alpha is mediated by indoleamine 2,3-dioxygenase. *Microbes Infect* 2004;6:806-812.
8. Mellor AL, Munn DH. IDO expression by dendritic cells: Tolerance and tryptophan catabolism. *Nat Rev Immunol* 2004;4:762-774.
9. Munn DH, Shafizadeh E, Attwood JT, Bondarev I, Pashine A, Mellor AL. Inhibition of T cell proliferation by macrophage tryptophan catabolism. *J Exp Med* 1999;189:1363-1372.
10. Munn DH, Sharma MD, Hou D, et al. Expression of indoleamine 2,3-dioxygenase by plasmacytoid dendritic cells in tumor-draining lymph nodes. *J Clin Invest* 2004;114:280-290.
11. Fallarino F, Grohmann U, Vacca C, et al. T cell apoptosis by tryptophan catabolism. *Cell Death Differ* 2002;9:1069-1077.
12. Frumento G, Rotondo R, Tonetti M, Damonte G, Benatti U, Ferrara GB. Tryptophan-derived catabolites are responsible for inhibition of T and natural killer cell proliferation induced by indoleamine 2,3-dioxygenase. *J Exp Med* 2002;196:459-468.
13. Terness P, Bauer TM, Röse L, et al. Inhibition of allogeneic T cell proliferation by indoleamine 2,3-dioxygenase-expressing dendritic cells: Mediation of suppression by tryptophan metabolites. *J Exp Med* 2002;196:447-457.
14. Dai W, Gupta SL. Regulation of indoleamine 2,3-dioxygenase gene expression in human fibroblasts by interferon-gamma. Upstream control region discriminates between interferon-gamma and interferon-alpha. *J Biol Chem* 1990;265:19871-19877.
15. Babcock TA, Carlin JM. Transcriptional activation of indoleamine dioxygenase by interleukin 1 and tumor necrosis factor alpha in interferon-treated epithelial cells. *Cytokine* 2000;12:588-594.
16. Hissong BD, Byrne GI, Padilla ML, Carlin JM. Upregulation of interferon-induced indoleamine 2,3-dioxygenase in human macrophage cultures by lipopolysaccharide, muramyl tripeptide, and interleukin-1. *Cell Immunol* 1995;160:264-269.
17. Górska R, Gregorek H, Kowalski J, Laskus-Perendyk A, Syczewska M, Madaliński K. Relationship between clinical parameters and cytokine profiles in inflamed gingival tissue and serum samples from patients with chronic periodontitis. *J Clin Periodontol* 2003;30: 1046-1052.
18. Ukai T, Mori Y, Onoyama M, Hara Y. Immunohistological study of interferon-gamma- and interleukin-4-bearing cells in human periodontitis gingiva. *Arch Oral Biol* 2001;46:901-908.
19. Graves DT, Cochran D. The contribution of interleukin-1 and tumor necrosis factor to periodontal tissue destruction. *J Periodontol* 2003;74:391-401.
20. Murakami S, Hino E, Shimabukuro Y, et al. Direct interaction between gingival fibroblasts and lymphoid cells induces inflammatory cytokine mRNA expression in gingival fibroblasts. *J Dent Res* 1999;78:69-76.
21. Preshaw PM, Schifferle RE, Walters JD. *Porphyromonas gingivalis* lipopolysaccharide delays human polymorphonuclear leukocyte apoptosis in vitro. *J Periodontal Res* 1999;34:197-202.
22. von Bubnoff D, Bausinger H, Matz H, et al. Human epidermal Langerhans cells express the immunoregulatory enzyme indoleamine 2,3-dioxygenase. *J Invest Dermatol* 2004;123:298-304.
23. Braun D, Longman RS, Albert ML. A two-step induction of indoleamine 2,3 dioxygenase (IDO) activity during dendritic-cell maturation. *Blood* 2005;106: 2375-2381.
24. MacKenzie CR, Heseler K, Muller A, Daubener W. Role of indoleamine 2,3-dioxygenase in antimicrobial defence and immuno-regulation: Tryptophan depletion versus production of toxic kynurenines. *Curr Drug Metab* 2007;8:237-244.
25. Sarkhosh K, Tredget EE, Li Y, Kilani RT, Uludag H, Ghahary A. Proliferation of peripheral blood mononuclear cells is suppressed by the indoleamine 2,3-dioxygenase expression of interferon-gamma-treated skin cells in a co-culture system. *Wound Repair Regen* 2003;11:337-345.
26. Ito M, Ogawa K, Takeuchi K, et al. Gene expression of enzymes for tryptophan degradation pathway is upregulated in the skin lesions of patients with atopic dermatitis or psoriasis. *J Dermatol Sci* 2004;36:157-164.
27. Kai S, Goto S, Tahara K, Sasaki A, Tone S, Kitano S. Indoleamine 2,3-dioxygenase is necessary for cytolytic activity of natural killer cells. *Scand J Immunol* 2004;59:177-182.
28. Ligam P, Manuelpillai U, Wallace EM, Walker D. Localisation of indoleamine 2,3-dioxygenase and kynurenine hydroxylase in the human placenta and decidua: Implications for role of the kynurenine pathway in pregnancy. *Placenta* 2005;26:498-504.
29. Okamoto A, Nikaido T, Ochiai K, et al. Indoleamine 2,3-dioxygenase serves as a marker of poor prognosis in gene expression profiles of serous ovarian cancer cells. *Clin Cancer Res* 2005;11:6030-6039.
30. Santoso DI, Rogers P, Wallace EM, Manuelpillai U, Walker D, Subakir SB. Localization of indoleamine 2,3-dioxygenase and 4-hydroxynonenal in normal and pre-eclamptic placentae. *Placenta* 2002;23:373-379.
31. Carlin JM, Borden EC, Sondel PM, Byrne GI. Interferon-induced indoleamine 2,3-dioxygenase activity in human mononuclear phagocytes. *J Leukoc Biol* 1989;45: 29-34.

32. Hwu P, Du MX, Lapointe R, Do M, Taylor MW, Young HA. Indoleamine 2,3-dioxygenase production by human dendritic cells results in the inhibition of T cell proliferation. *J Immunol* 2000;164:3596-3599.
33. Robinson CM, Shirey KA, Carlin JM. Synergistic transcriptional activation of indoleamine dioxygenase by IFN-gamma and tumor necrosis factor-alpha. *J Interferon Cytokine Res* 2003;23:413-421.
34. van Wissen M, Snoek M, Smids B, Jansen HM, Lutter R. IFN-gamma amplifies IL-6 and IL-8 responses by airway epithelial-like cells via indoleamine 2,3-dioxygenase. *J Immunol* 2002;169:7039-7044.
35. Chaves AC, Ceravolo IP, Gomes JA, Zani CL, Romanha AJ, Gazzinelli RT. IL-4 and IL-13 regulate the induction of indoleamine 2,3-dioxygenase activity and the control of *Toxoplasma gondii* replication in human fibroblasts activated with IFN-gamma. *Eur J Immunol* 2001;31:333-344.
36. Carlin JM, Weller JB. Potentiation of interferon-mediated inhibition of *Chlamydia* infection by interleukin-1 in human macrophage cultures. *Infect Immun* 1995; 63:1870-1875.
37. Wirleitner B, Reider D, Ebner S, et al. Monocyte-derived dendritic cells release neopterin. *J Leukoc Biol* 2002;72:1148-1153.
38. Munn DH, Sharma MD, Mellor AL. Ligation of B7-1/B7-2 by human CD4+ T cells triggers indoleamine 2,3-dioxygenase activity in dendritic cells. *J Immunol* 2004;172:4100-4110.
39. Mahanonda R, Sa-Ard-Iam N, Montreekachon P, et al. IL-8 and IDO expression by human gingival fibroblasts via TLRs. *J Immunol* 2007;178:1151-1157.

Correspondence: Dr. Kanokwan Nisapakultorn, Department of Periodontology, Chulalongkorn University, 34 Henri-Dunant Road, Patumwan, Bangkok, 10330, Thailand. Fax: 66-2-218-8851; e-mail: nisa0003@hotmail.com.

Submitted June 10, 2008; accepted for publication July 28, 2008.

THE JOURNAL OF BIOLOGICAL CHEMISTRY VOL. 284, NO. 46, pp. 31914–31920, November 13, 2009

Aβ42-to-Aβ40- and Angiotensin-converting Activities in Different Domains of Angiotensin-converting Enzyme*

Received for publication, April 21, 2009, and in revised form, September 3, 2009 Published, JBC Papers in Press, September 22, 2009, DOI 10.1074/jbc.M109.011437

Kun Zou[‡1], Tomoji Maeda[‡], Atsushi Watanabe[§], Junjun Liu[‡], Shuyu Liu[‡], Ryutaro Oba[¶], Yoh-ichi Satoh[‖], Hiroto Komano[‡2], and Makoto Michikawa[3]**

*From the [‡]Department of Neuroscience, School of Pharmacy, and the [‖]Department of Anatomy, School of Medicine, Iwate Medical University, 2-1-1 Nishitokuda, Yahaba, Iwate 028-3694, Japan, the [¶]Department of Advanced Medicine and Development, BML, Inc., 1361-1 Matoba, Kawagoe, Saitama 350-1101, Japan, and the Departments of [§]Vascular Dementia Research and **Alzheimer Disease Research, National Institute for Longevity Sciences, National Center for Geriatrics and Gerontology, 36-3 Gengo, Morioka, Obu, Aichi 474-8522, Japan*

Amyloid β-protein 1–42 (Aβ42) is believed to play a causative role in the development of Alzheimer disease (AD), although it is a minor part of Aβ. In contrast, Aβ40 is the predominant secreted form of Aβ and recent studies have suggested that Aβ40 has neuroprotective effects and inhibits amyloid deposition. We have reported that angiotensin-converting enzyme (ACE) converts Aβ42 to Aβ40, and its inhibition enhances brain Aβ42 deposition (Zou, K., Yamaguchi, H., Akatsu, H., Sakamoto, T., Ko, M., Mizoguchi, K., Gong, J. S., Yu, W., Yamamoto, T., Kosaka, K., Yanagisawa, K., and Michikawa, M. (2007) *J. Neurosci.* 27, 8628–8635). ACE has two homologous domains, each having a functional active site. In the present study, we identified the domain of ACE, which is responsible for converting Aβ42 to Aβ40. Interestingly, Aβ42-to-Aβ40-converting activity is solely found in the N-domain of ACE and the angiotensin-converting activity is found predominantly in the C-domain of ACE. We also found that the *N*-linked glycosylation is essential for both Aβ42-to-Aβ40- and angiotensin-converting activities and that unglycosylated ACE rapidly degraded. The domain-specific converting activity of ACE suggests that ACE inhibitors could be designed to specifically target the angiotensin-converting C-domain, without inhibiting the Aβ42-to-Aβ40-converting activity of ACE or increasing neurotoxic Aβ42.

Angiotensin-converting enzyme (ACE)[4] plays a key role in the renin-angiotensin system (RAS), which is involved in the long-term regulation of blood pressure and blood volume in the human body. Recent genetic, pathologic, and biochemical studies have associated ACE with onset of Alzheimer disease (AD) (1, 2). The I allele of the *ACE* gene, which results in a reduced serum ACE level, has been demonstrated to be associated with AD (3–5). Hypertension is a risk factor for AD and ACE inhibitors for treatment of hypertension were shown to be the only drug class among the antihypertensives to potentially be associated with a slight increased incidence of AD (adjusted hazard ratio 1.13) (6, 7). A mechanistic link between ACE and AD was suggested when ACE was shown to degrade Aβ40 and Aβ42 (8, 9). Overexpression of Aβ40 in transgenic mice does not cause brain amyloid deposition, the major pathological hallmark of AD, whereas expression of Aβ42 is shown to be essential for amyloid deposition (10, 11). In addition, Aβ40 has an inhibitory effect on amyloid deposition *in vitro* and *in vivo* and has neuroprotective effects (12–14). These lines of evidence suggest that converting Aβ42 to Aβ40 may be a potential strategy for development of an AD therapy. In our previous study, we identified ACE as an Aβ42-to-Aβ40-converting (Aβ-converting) enzyme and showed that ACE inhibitor enhances brain Aβ42 deposition in transgenic mice (15). Clarifying the molecular base of ACE domain-specific enzymatic activity on Aβ42 to Aβ40 conversion, Aβ degradation, and angiotensin conversion emerges to be important for development of a strategy for hypertension and AD treatment.

ACE is a type I integral membrane glycoprotein, and there are two isoforms of ACE in mammals that arise from the use of alternative promoters in a single gene: somatic ACE and testicular ACE. ACE also has one mammalian relative, ACE2, which consists of a single active site domain that, by sequence comparison, more closely resembles the N-domain than the C-domain of somatic ACE. ACE converts angiotensin I to angiotensin II, a potent vasoconstrictor, and inactivates bradykinin, a vasodilator (16). Given the central role ACE plays in regulation of blood pressure, ACE inhibitors are widely used for the treatment of hypertension in the elderly population. ACE also hydrolyzes a wide range of polypeptide substrates, including substance P, luteinizing hormone-releasing hormone, acetyl-Ser-Asp-Lys-Pro (AcSDKP), and neurotensin (16). The mammalian somatic ACE contains two homologous domains, the N-terminal domain (N-domain) and C-terminal domain (C-domain), each bearing a zinc-dependent active site. The pres-

* This work was supported by grants from the Ministry of Education, Culture, Sports, Science and Technology of Japan, Grant-in-Aid for Young Scientists (Start-up) (19800040), and Scientific Research (B) (19300138), the Ministry of Health, Labor and Welfare of Japan (Comprehensive Research on Aging and Health) (H20-007), the Program for Promotion of Fundamental Studies in Health of the National Institute of Biomedical Innovation (NIBIO), Takeda Science Foundation, Kato Memorial Bioscience Foundation, and The Ichiro Kanehara Foundation for the Promotion of Medical Sciences and Medical Care.

[1] To whom correspondence may be addressed. Tel.: 81-19-698-1820; Fax: 81-19-698-1864; E-mail: kunzou@iwate-med.ac.jp.

[2] To whom correspondence may be addressed. Tel.: 81-19-698-1820; Fax: 81-19-698-1864; E-mail: hkomano@iwate-med.ac.jp.

[3] To whom correspondence may be addressed. Tel.: 81-562-46-2311; Fax: 81-562-46-8569; E-mail: michi@nils.go.jp.

[4] The abbreviations used are: ACE, angiotensin-converting enzyme; Aβ, amyloid β-protein; F-ACE, full-domain ACE; N-ACE, N-terminal domain ACE; C-ACE, C-terminal domain ACE; MALDI-TOF-MS, matrix-assisted laser desorption ionization-time of flight-mass spectrometry; AD, Alzheimer Disease.

ence of two active sites in ACE has stimulated many attempts to establish whether they differ in function. For example, AcSDKP, a peptide suggested to inhibit bone marrow maturation, is found to be preferentially cleaved by the N-domain of ACE *in vitro* (17). In contrast, the ACE C-domain is demonstrated to be the main site of angiotensin I cleavage *in vivo* (18). The *N*-linked glycosylation of testicular ACE, a homologue of the somatic ACE N-domain, is essential for its enzymatic activity and for preventing degradation (19).

In our current study, we determined the contributions of each ACE domain, toward Aβ42-to-Aβ40- and/or angiotensin-converting activity. We postulated that the dipeptidyl carboxypeptidase activity of ACE, which converts angiotensin I to angiotensin II and Aβ42 to Aβ40, is located in its C-domain. Surprisingly, we found that the Aβ42-to-Aβ40-converting activity is specifically in the N-domain of ACE, and the angiotensin-converting activity is predominantly in the C-domain of ACE. We also found that both Aβ42-to-Aβ40- and angiotensin-converting activities require the *N*-linked glycosylation of ACE. The finding of domain-specific Aβ42-to-Aβ40-converting activity of ACE may help design a domain-specific ACE inhibitor for treatment of hypertension, without inhibiting the N-domain-specific Aβ42-to-Aβ40-converting activity of ACE.

EXPERIMENTAL PROCEDURES

Truncated ACE Expression and Purification—Expression and purification of ACE recombinant proteins were carried out as described previously (20). Mutated ACE cDNAs containing two active domains (F-ACE) or only the N-terminal active domain or C-terminal active domain (N-ACE or C-ACE) were cloned into pcDNA3.1(-) vectors (Invitrogen). Six histidine residues were introduced at the C-terminal end of each cDNA. The C-terminal transmembrane domain was removed from all of the recombinant ACE proteins to allow them to be secreted into the culture medium. COS7 cells were grown in Dulbecco's modified Eagle's medium (DMEM) containing 10% fetal bovine serum. Transfections of the ACE pcDNA3.1(-) vectors in COS7 cells were performed using Lipofectamine 2000 (Invitrogen), and COS7 cells stably expressing F-, N-, and C-ACE were selected in DMEM containing 10% fetal bovine serum and 1 mg/ml Geneticin (Wako, Japan). Culture media were harvested 3 days after the cells reached confluence, and recombinant ACE proteins were purified using a TALON purification kit (Clontech). The purified proteins were then dialyzed in 50 mM HEPES, 50 mM NaCl, 1 μM $ZnCl_2$, pH 7.5 and concentrated with Centricon YM-50 (Millipore). Protein concentrations of the ACE proteins were determined using a BCA protein assay kit (Pierce).

Western Blot Analysis and Determining Conversion of Aβ42 to Aβ40—COS7 cells were lysed in radioimmune precipitation assay buffer (10 mM Tris/HCl (pH 7.5), 150 mM NaCl, 1% Nonidet P-40, 0.1% sodium dodecyl sulfate (SDS), and 0.2% sodium deoxycholate, containing a protease inhibitor mixture (Roche Applied Science)). The expression of ACE recombinant proteins was detected by Western blotting using a polyclonal anti-ACE antibody (R&D). Aβ1–42 (Peptide Institute) was freshly dissolved in 0.1% $NH_3 \cdot H_2O$ at 200 μM for each experiment. 80 μl of F-, N-, and C-ACE at a concentration of 0.5 μM were mixed with synthetic Aβ42 to a final concentration of 40 μM and incubated at 37 °C. 10 μl of the mixture was subjected to SDS-PAGE and blotted on a nitrocellulose membrane. To enhance the reactivity to an anti-Aβ40 antibody, the membrane was boiled in PBS for 3 min after blotting, probed with an anti-Aβ40 monoclonal antibody (1A10) (IBL), and visualized with SuperSignal (Pierce). Because of the high level of exogenous Aβ42, the membrane was not boiled before the reaction with a polyclonal anti-Aβ42 antibody. The quantitation of Aβ40 generation and Aβ42 degradation was carried out using Image J 1.41 software (NIH).

ACE Activity Assay—F-ACE, N-ACE, and C-ACE were dialyzed in 50 mM HEPES, 50 mM NaCl, 1 μM $ZnCl_2$, pH 7.5, and their activities against the synthetic substrate *N*-hippuryl-l-histidyl-l-leucine (Hip-His-Leu) were determined using an ACE colorimetric kit (Buhlmann Laboratories, Schonenbuch, Switzerland). 10 μl of ACE proteins at a concentration of 0.5 μM were mixed and incubated with ACE substrate at 37 °C. The reaction time was 15 min. All samples were measured in triplicate.

Mass Spectrometry Analysis—Purified F-ACE, N-ACE, or C-ACE was incubated with 80 μM Aβ42 at 37 °C for 2 h. Captopril (10 μM) was added to stop digestion, and the sample was frozen in −80 °C until use. The samples were mixed with 3,5-dimethoxy-4-hydroxycinnamic acid (Wako, Japan) as a matrix, and then subjected to matrix-assisted laser desorption ionization-time of flight-mass spectrometry (MALDI-TOF-MS) (AXIMA-CFR, SHIMADZU, Kyoto, Japan) to detect the generation of Aβ40 and other Aβ fragments. The same amount of F-ACE, N-ACE, C-ACE, or Aβ42 incubated alone under the same conditions as described above was used as control.

Expression of ACE Active Site Mutants and Determining Their Domain-specific Activities—The pcDNA5/FRT expression vectors bearing the catalytically inactive full-length ACE were kindly provided by Dr. Dennis J. Selkoe (9). The two ACE zinc metalloprotease active site glutamates (amino acids 362 in the N-domain and 960 in the C-domain) were changed to aspartates. Mouse embryonic fibroblasts at 90% confluence were transiently transfected with the vectors bearing ACE full-length protein with active site mutations using Lipofectamine 2000 (Invitrogen). After 48 h, the cells were lysed in in 50 mM Tris/HCl (pH 7.5) containing 0.5% Nonidet P-40, and nuclei and cell debris was pelleted at 10,000 × *g* for 10 min at 4 °C. To assay ACE activity, 5 μg of protein of cell lysate was incubated with Hip-His-Leu. For the Aβ42-to-Aβ40-converting activity assay, ACE in each cell lysate was immunoprecipitated using a polyclonal anti-ACE antibody (R&D) and protein G-Sepharose (GE Healthcare). Immunoprecipitated ACE was then incubated with 40 μM synthetic Aβ42 at 37 °C for 15 h. Captopril (10 μM) was added to the mixture to stop the reaction and the conversion of Aβ40 from Aβ42 was detected by Western blot.

Deglycosylation of ACE Proteins—To assess the type of glycosylation of human kidney ACE and recombinant ACE proteins, the ACE proteins were treated with PNGase F, *O*-glycanase, or sialidase A using an enzymatic deglycosylation kit according to the manufacturer's instructions (PROzyme, San Leandro, CA). To evaluate the enzymatic activities of deglycosylated ACE proteins, non-denaturing protocol was used, and ACE proteins

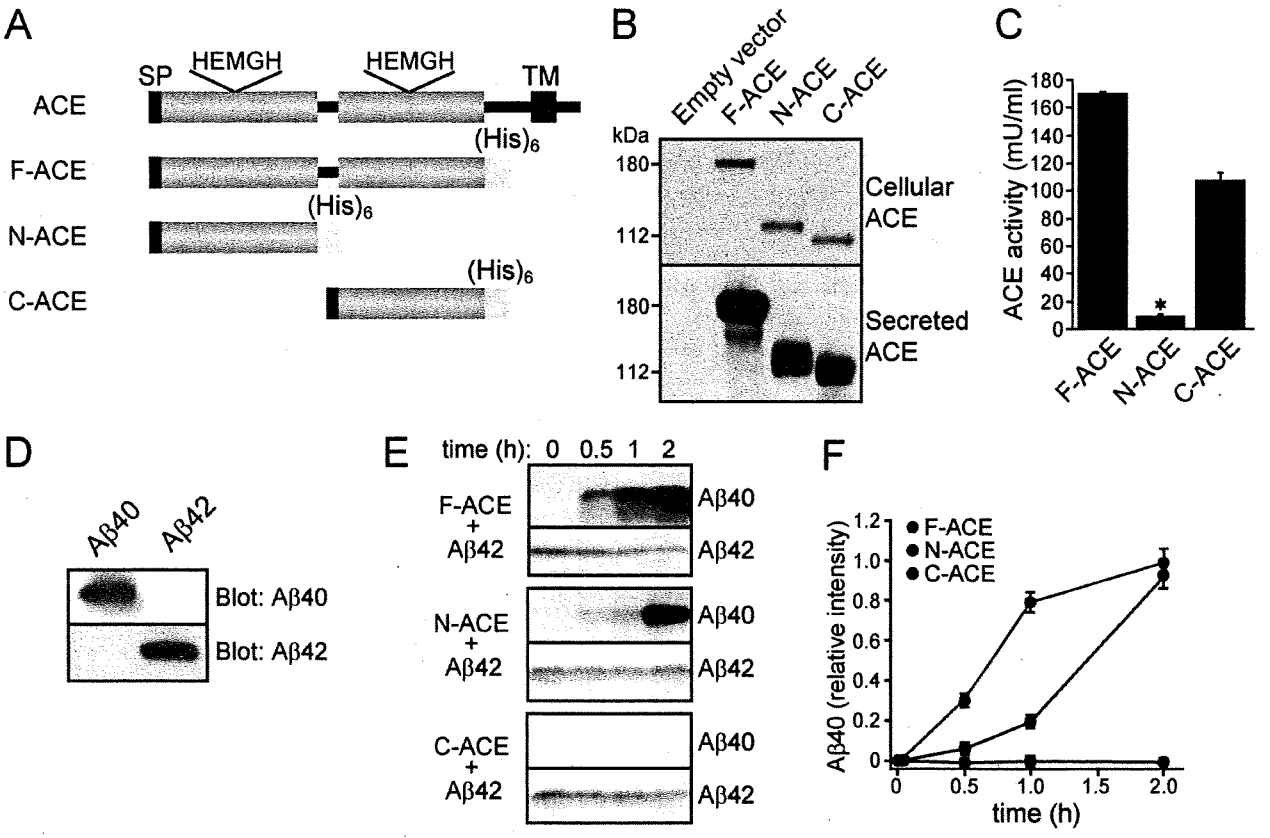

FIGURE 1. **Identification of N-domain-specific Aβ42-to-Aβ40-converting activity of ACE.** *A*, schematic representation of the human ACE and recombinant ACE proteins. The wild-type ACE protein contains a signal peptide (*SP*), a single transmembrane domain (*TM*), and two homologous catalytic domains (*light blue box*). Recombinant ACE proteins, F-ACE, N-ACE, and C-ACE, contain 6 histidine residues (*yellow box*) at the C terminus and a signal peptide at the N terminus. *B*, COS7 cells transfected with empty vector or cells stably expressing F-ACE, N-ACE, or C-ACE were lysed in radioimmune precipitation assay buffer. Western blots of 20 μg of total protein from the cells or 2 μg of ACE isolated from the culture medium were probed with a polyclonal anti-ACE antibody. *C*, ACE activity was measured by incubating 0.5 μM F-ACE, N-ACE, or C-ACE with the substrate Hip-His-Leu for 15 min at 37 °C. N-ACE has markedly reduced ACE activity compared with C-ACE. Values represent the means + S.E.; $n = 3$; *, $p < 0.001$, Bonferroni/Dunn test. *D*, specificities of monoclonal anti-Aβ40 (1A10) and polyclonal anti-Aβ42 antibodies were confirmed by Western blot of 0.1 μg of Aβ40 and Aβ42. *E*, F-, N-, and C-ACE were mixed with synthetic Aβ42 and incubated at 37 °C for 0.5, 1, or 2 h. Western blots of the mixture were probed with anti-Aβ40 and anti-Aβ42 antibodies. In contrast to the ACE activity, the Aβ42-to-Aβ40-converting activity was solely detected in N-ACE. *F*, generation of Aβ40 and the degradation of Aβ42 were determined by densitometry.

were deglycosylated at 37 °C for 1 h. The non-deglycosylated ACE proteins were mixed with the same incubation buffer provided by the manufacturer and incubated except that glycosidases were not added.

RESULTS

ACE N-domain, but Not C-domain, Converts Aβ42 to Aβ40—To explore which domain of ACE has Aβ42-to-Aβ40-converting activity, we prepared 3 kinds of recombinant ACE proteins, which were transfected into COS7 cells. F-ACE contains both the N-domain and C-domain active sites. N-ACE contains only the N-terminal active site, and C-ACE only contains the C-terminal active site. All three kinds of mutated ACE were fused with a 6-histidine tag at the C-terminal for the isolation from the culture medium (Fig. 1*A*). Cell lines stably expressing F-ACE, N-ACE, or C-ACE were selected by Geneticin and the expression of the ACE-mutated proteins were confirmed by Western blot. The endogenous ACE was not detected in the cell lysate of COS7 cells transfected with empty vectors. F-, N-, and C-ACE showed molecular masses at 180, 130, and 110 kDa, respectively (Fig. 1*B*). The secreted ACE recombinant proteins were isolated from the culture medium by immobilized metal chromatography. The proteins were then dialyzed and concentrated. The apparent molecular mass of each secreted ACE recombinant protein did not differ from each of the cellular ACE recombinant proteins (Fig. 1*B*). ACE enzymatic activity of the F-ACE, N-ACE, and C-ACE was confirmed by degradation of the substrate Hip-His-Leu (Fig. 1*C*). F-ACE was found to have the highest Hip-His-Leu-degrading activity and C-ACE had 63% ACE activity compared with F-ACE, whereas N-ACE had a significantly reduced ACE activity, confirming the finding of the ACE C-domain as the main site of angiotensin I cleavage *in vivo* (18) (Fig. 1*C*).

We have found that ACE releases two amino acids from the C terminus of Aβ42 and generates Aβ40. Aβ1–41 was not found during the degradation of Aβ42 by ACE, suggesting that the Aβ42-to-Aβ40-converting activity of ACE is a dipeptidyl carboxypeptidase enzymatic activity (15). To determine which domain is responsible for the Aβ42-to-Aβ40-converting activity, we incubated Aβ42 with F-ACE, N-ACE, or C-ACE and examined the generation of Aβ40 from Aβ42 by Western blot using anti-Aβ40- and anti-Aβ42-specific antibodies. The specificity of the two antibodies was examined by Western blotting of synthetic Aβ40 and Aβ42, and cross reaction between these

two antibodies was not found (Fig. 1*D*). Unexpectedly, in contrast to the angiotensin-converting activity, the Aβ42-to-Aβ40-converting activity was found in F-ACE and N-ACE, but not in C-ACE, indicating that N-domain of ACE has the Aβ42-to-Aβ40-converting activity. Although C-ACE showed a similar Aβ42-degrading activity compared with F-ACE and N-ACE, it did not generate Aβ40 from Aβ42 (Fig. 1*E*). Incubation of C-ACE with Aβ42 up until 16 h did not generate Aβ40 (data not shown). F-ACE generated more Aβ40 from Aβ42 than N-ACE at the time points of 0.5 and 1 h, whereas at the time point of 2 h F-ACE and N-ACE generated similar amounts of Aβ40 (Fig. 1, *E* and *F*). F-ACE had similar activities compared with native human kidney ACE regarding the Aβ42-to-Aβ40-converting activity and the Hip-His-Leu-degrading activity (Figs. 1*E* and 4*C* and data not shown).

To determine other products other than Aβ40 that were generated by ACE from Aβ42 and to confirm the result from Western blot, we performed mass spectrometry analysis. Consistent with our immunological studies, a peak corresponding to Aβ1–40 was detected in the F-ACE- and N-ACE-digested samples; in addition, F-ACE and N-ACE also generated peaks corresponding to Aβ1–33, Aβ1–28, Aβ1–24, and Aβ1–21 from Aβ42, whereas Aβ1–40 was not formed by C-ACE. However, C-ACE generated four other Aβ fragments, Aβ1–33, Aβ1–28, Aβ1–24, and Aβ1–21 (Fig. 2*A*). Mass spectrometry analysis for incubated F-ACE, N-ACE, or C-ACE alone did not show any Aβ peptide signal, and synthetic Aβ42 only showed one peak with a mass at 4514, which matched the predicted mass of Aβ1–42 (Fig. 2*B* and data not shown). These results from mass spectrometry confirmed that the Aβ42-to-Aβ40-converting activity is restricted to the ACE N-domain.

N-domain-inactive ACE Mutant Loses Aβ42-to-Aβ40-converting Activity—Three ACE mutants were generated by site-directed mutagenesis to change the active site sequence HEMGH to HDMGH in N-, C-, or both N- and C-domain. The N-domain active site was inactivated by mutating glutamate 362 to aspartate (termed E362D), and the C-domain active site was similarly inactivated by mutating glutamate 960 to aspartate (termed E960D). E362/960D has double mutations in its N- and C-domain active sites (Fig. 3*A*). The fibroblasts were transiently transfected with empty vector or ACE mutant constructs. ACE was not detected in the fibroblasts transfected with empty vector, and wtACE and ACE mutants were expressed in the cells at a similar level (Fig. 3*B*). To determine the effects of each ACE active site on ACE activity, cell lysate from each cell lines was analyzed for ACE activity. Consistent with our results from purified truncated ACE proteins, E362D containing only the C-domain active site has the similar ACE activity compared with wtACE, whereas E960D has an extremely low ACE activity. ACE inhibitor, captopril, completely inhibited this ACE activity (Fig. 3*C*). To determine which active site in each domain is responsible for the Aβ42-to-Aβ40-converting activity, wtACE and ACE mutant proteins were immunoprecipitated and incubated with Aβ42. A similar amount of immunoprecipitated ACE was confirmed by Western blotting (Fig. 3*D*, *upper panel*). E960D without the C-domain activity generated similar amount of Aβ40 from Aβ42 compared with

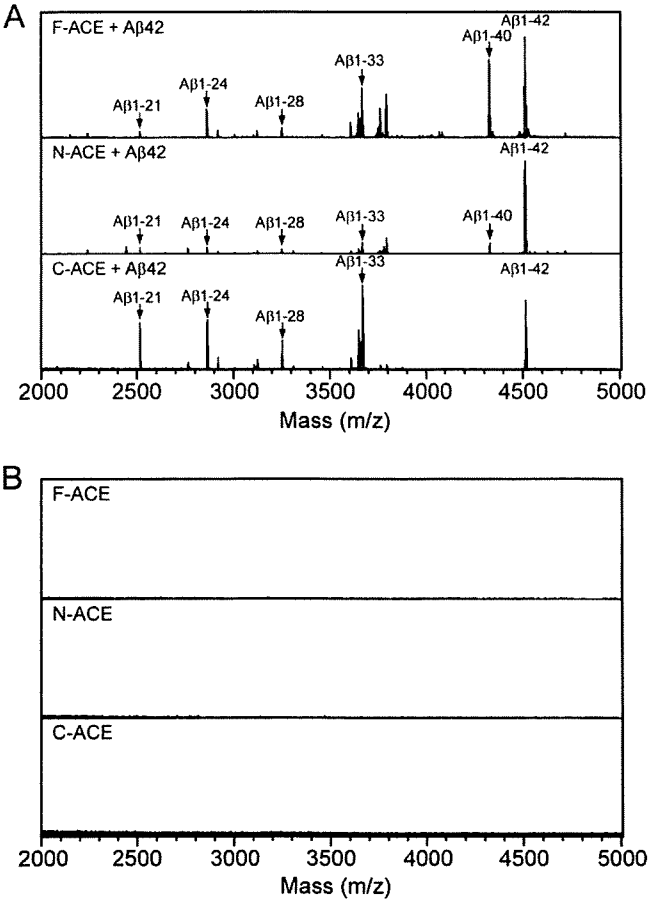

FIGURE 2. **MALDI-TOF-MS analysis for Aβ42 degradation by F-ACE, N-ACE, or C-ACE.** *A*, Aβ42 (80 μM) was incubated with 0.5 μM purified F-ACE, N-ACE, or C-ACE at 37 °C for 2 h, then captopril (10 μM) was added after incubation to stop the digestion. 1 μl of the mixture was subjected to MALDI-TOF-MS analysis. F-ACE and N-ACE generated Aβ1–40, whereas C-ACE did not. *B*, 1 μl of F-ACE, N-ACE, or C-ACE alone incubated at 37 °C for 2 h was subjected to MALDI-TOF-MS analysis, and a peptide signal was not detected.

wtACE, whereas E362D and E362/960D without N-domain activity did not convert Aβ42 to Aβ40 (Fig. 3*D*, *middle panel*).

N-Glycosylation Is Essential for Aβ42-to-Aβ40- and Angiotensin-converting Activities—ACE is a glycoprotein, and the *N*-linked glycosylation of testicular ACE has been shown to be essential for its angiotensin-converting activity. Human ACE has 17 putative Asn*X*(Ser/Thr) *N*-linked glycosylation sites distributed throughout both the N-domain and C-domain (21). To determine the role of glycosylation of ACE in its enzymatic activities and to compare the glycosylation of natural human ACE with that of recombinant F-ACE, N-ACE, and C-ACE, we examined the type of glycosylation of these ACE proteins by the treatment with PNGase F, *O*-glycanase, and sialidase A. Treatment with PNGase F, *O*-glycanase, and sialidase A remarkably reduced the molecular weight of human kidney ACE, F-ACE, N-ACE, and C-ACE (Fig. 4*A*, *lanes 1* and *2*). Removal of *N*-linked glycosylation using PNGase F alone produced similar molecular weight shifts, whereas *O*-glycanase did not produce any shift in ACE size (Fig. 4*A*, *lanes 3* and *4*). The sensitivity of N-ACE to PNGase F indicates that N-ACE is modified by *N*-linked glycosylation. All the ACE proteins showed a slight decrease in the molecular weight after sialidase A digestion,

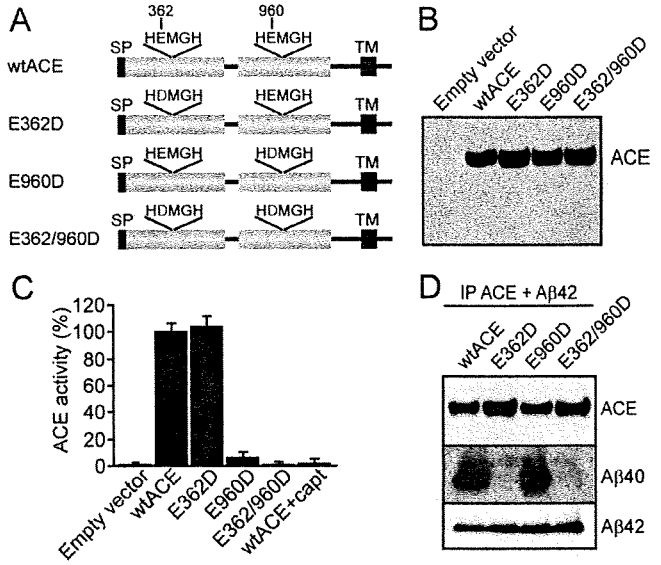

FIGURE 3. **Site-directed mutated ACE proteins exhibit domain-specific Aβ42-to-Aβ40- and angiotensin-converting activity.** *A*, schematic representation of human ACE and the mutant positions. The two ACE zinc metalloprotease active site glutamates (amino acids 362 in the N-domain and 960 in the C-domain) were changed to aspartates. *B*, fibroblasts were transiently transfected with empty vector, wtACE or mutant ACE plasmids and the expression of ACE proteins was detected by Western blotting using a polyclonal anti-ACE antibody. *C*, ACE activity was measured by incubating 5 μg of protein of cell lysate with the substrate Hip-His-Leu for 10 min at 37 °C. ACE activity in cell lysate was clearly detected in wtACE and E362D. C-domain inactive ACE protein, E960D, showed an extremely low ACE activity; and double mutants in both domains of ACE, E362/960D, did not show ACE activity. ACE activity was clearly inhibited by captopril (1 μM) treatment. *D*, ACE in cell lysate (4 mg of protein) from each transfected cell line was immunoprecipitated by 5 μg of polyclonal anti-ACE antibody and 100 μl of protein G-Sepharose. Immunoprecipitated ACE was then incubated with synthetic Aβ42 and the generation of Aβ40 was detected by Western blotting. *SP*, signal peptide; *TM*, transmembrane.

indicating the sialylation of their *N*-glycans (Fig. 4*A*, *lane 5*). These results suggest that the glycosylation type of natural human kidney ACE and recombinant ACE proteins produced by COS7 cells are identical. Because ACE is modified by *N*-linked glycosylation and *O*-linked glycosylation was not detected, we used PNGase to remove its *N*-glycans and studied the ACE activity. As expected, PNGase-treated human kidney ACE showed a 96% reduced ACE activity in degradation of Hip-His-Leu compared with untreated ACE (Fig. 4*B*).

To determine the role of *N*-linked glycosylation of ACE in its Aβ42-to-Aβ40-converting activity, we incubated Aβ42 with PNGase F-treated or untreated human kidney ACE and examined Aβ40 generation by Western blot. Deglycosylated human kidney ACE showed a decreased molecular mass at ~150 kDa and was degraded by itself after 2 h of incubation. After incubation for 16 h, ~150-kDa deglycosylated ACE was completely degraded (Fig. 4*C*, *upper panel*). Aβ40 was generated from Aβ42 by ACE after incubating the mixture of Aβ42 and ACE for 15 min. The level of Aβ40 increased in a time-dependent manner and reached a peak after incubation for 2 h, whereas deglycosylated ACE did not generate Aβ40 from Aβ42, although it showed a similar Aβ42-degrading activity compared with non-deglycosylated ACE (Fig. 4*C*, *middle and bottom panels*). This glycosylation-required Aβ42-to-Aβ40-converting activity was also confirmed in recombinant ACE proteins. PNGase F-deglycosylated F-ACE, N-ACE, and C-ACE have similar Aβ42-degrading activity. However, deglycosylated F-ACE and N-ACE failed to generate Aβ40 from Aβ42, suggesting that the *N*-linked glycosylation in the ACE N-domain is essential for its Aβ42-to-Aβ40-converting activity (Fig. 4*D*). Sialidase A treatment did not change the Aβ42-to-Aβ40-converting activity and the ACE activity of human kidney ACE, indicating that sialylation is not required for its activities (data not shown).

Captopril and Enalaprilat Showed Different IC_{50} on Aβ42-to-Aβ40-converting Activity—The feature of ACE inhibitors has been well studied in terms of their angiotensin-converting inhibitory effect. To explore whether ACE inhibitors differentially inhibit the Aβ42-to-Aβ40-converting activity, we determined the IC_{50} of captopril, perindopril, lisinopril, and enalaprilat toward the angiotensin- and Aβ42-to-Aβ40-converting activity of F-ACE. All four ACE inhibitors showed a similar IC_{50} on the inhibition of angiotensin-converting activity of F-ACE, whereas enalaprilat exhibited a 10-fold lower IC_{50} (0.003~0.01 μM) on Aβ42-to-Aβ40-converting activity than captopril (0.03~0.1 μM) (Table 1).

DISCUSSION

Most mammalian tissues contain ACE with two catalytic domains. Evolutionary conservation of the ACE N- and C-domains suggests important distinct functions of these domains. Recent genetic studies have associated the I allele of the *ACE* gene, which results in a reduced serum ACE level, with onset of AD (1, 3). We have shown previously that ACE converts Aβ42 to Aβ40, and its inhibition predominantly enhances brain Aβ42 deposition (15). To investigate which domain of ACE is responsible for Aβ42-to-Aβ40-converting activity and whether ACE inhibitors inhibit this activity, we generated three kinds of ACE proteins, containing both N- and C-domains or containing either single active domain. We also used selective site-directed mutagenesis of ACE to study the domain-specific activity of full-length ACE. The present study shows that the Aβ42-to-Aβ40- and angiotensin-converting activities were located in different ACE domains and that *N*-linked glycosylation was essential for the two ACE enzymatic activities. The N-domain of ACE clearly showed an Aβ42-to-Aβ40-converting activity, whereas it has an extremely low angiotensin-converting activity. In contrast, the C-domain of ACE showed angiotensin-converting activity, whereas the Aβ42-to-Aβ40-converting activity was not detected in this domain.

In a cellular context, both the N-domain and C-domains of ACE are able to degrade Aβ40 and Aβ42 (9). In our studies, we also found that the N- and C-domains were indistinguishable as regarding degrading Aβ42, suggesting that both N- and C-domains of ACE have endopeptidase activity for Aβ42. In the overall scheme of Aβ42 processing, the full-length ACE cleaving into many fragments may be important for therapeutic treatment of AD. We showed that Aβ40, but not Aβ41, was generated from Aβ42 (Fig. 2*A*). However, the Aβ42-to-Aβ40-converting activity was solely found in the N-domain of ACE (Figs. 1, 2, and 3). These results suggest that the dipeptidyl carboxypeptidase activity converting Aβ42 to Aβ40 is restricted to its N-domain. The N-domain specific dipeptidyl activity was

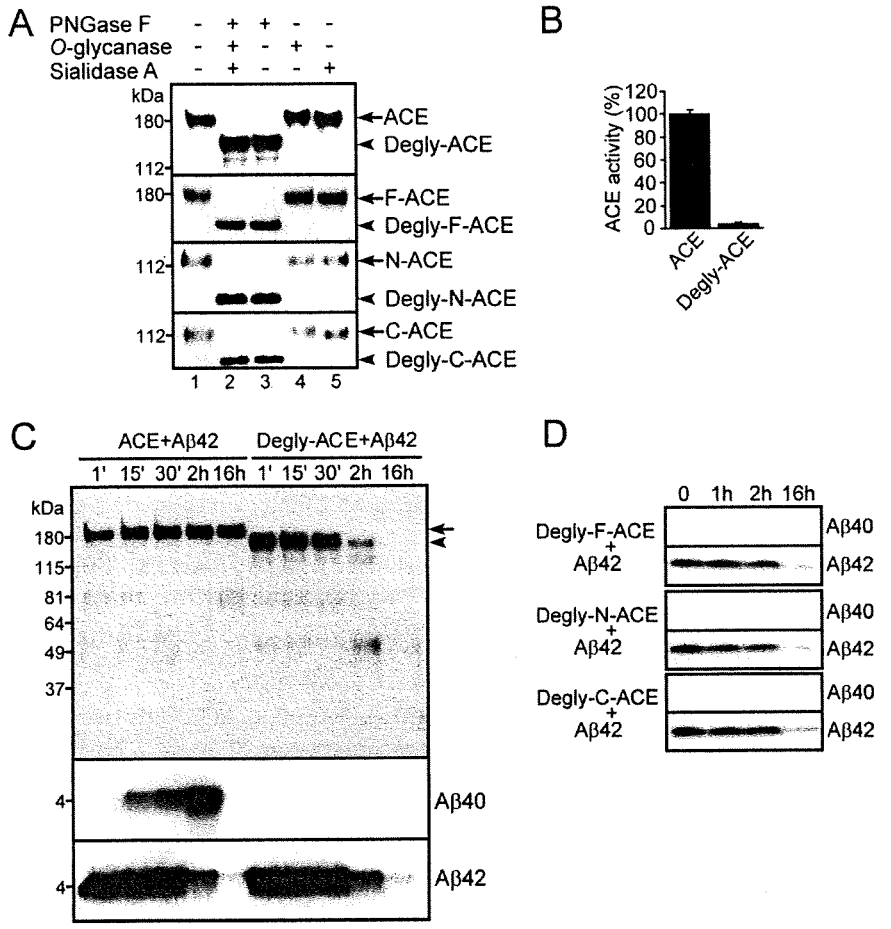

FIGURE 4. **Characterization of ACE glycosylation and role of the glycosylation in ACE activity and Aβ42-to-Aβ40-converting activity.** *A*, 5 μg of purified human kidney ACE, F-ACE, N-ACE, and C-ACE were deglycosylated with 1 μl of PNGase F, *O*-glycanase, and/or sialidase A for 1 h at 37 °C. PNGase F alone was able to remove all glycosylation of ACE. *B*, ACE activity of PNGase F-deglycosylated human kidney ACE was measured immediately after deglycosylation using an ACE colorimetric kit. ACE activity was almost completely abolished by *N*-deglycosylation. *C*, 80 μl of human kidney ACE (0.5 μM) with or without *N*-deglycosylation was mixed with synthetic Aβ42 (40 μM) and incubated at 37 °C. 10 μl of the mixture were collected at various incubation time points and subjected to Western blot analysis. Deglycosylated ACE showed no Aβ42-to-Aβ40-converting activity, whereas the Aβ42-degrading activity remained. *D*, 40 μl of recombinant F-, N-, and C-ACE proteins (0.5 μM) were deglycosylated and mixed with Aβ42 and incubated at 37 °C for 1, 2, or 16 h. Aβ42-to-Aβ40-converting activity was not detected in either deglycosylated F-ACE or deglycosylated N-ACE, whereas all the deglycosylated ACE showed an Aβ42-degrading activity.

TABLE 1

ACE inhibitors inhibited Aβ42-to-Aβ40-converting activity with different IC_{50}

ACE activity of 10 μl of F-ACE (0.5 μM) was measured using an ACE colorimetric kit, and Aβ42-to-Aβ40-converting activity was measured by Western blotting and densitometry. 0, 0.003, 0.01, 0.03, 0.1, 0.3, 1, 3, 10 μM ACE inhibitors were added to determine the IC_{50} for Aβ42-to-Aβ40-converting activity.

ACE inhibitors	ACE activity IC_{50}	Aβ-converting activity IC_{50}[a]
	μM	μM
Captopril	0.01–0.03	0.03–0.1
Enalaprilat	0.01–0.03	0.003–0.01
Lisinopril	0.01–0.03	0.01–0.03
Perindopril	0.03–0.1	0.01–0.03

[a] Aβ-converting activity, Aβ42-to-Aβ40-converting activity.

also found in the degradation of AcSDKP, which is involved in the control of hematopoietic stem cell proliferation. The molecular basis in which the N-domain of ACE accesses AcSDKP and Aβ42 remains to be elucidated. The N- and C-domains of ACE have reduced Aβ42-to-Aβ40-converting activity and angiotensin-converting activity, respectively, compared with full domain ACE (Fig. 1, *C* and *F*), suggesting that each catalytic domain of ACE regulates the activity of the other, and both domains are required for normal substrate recognition and degradation. Mice with a selective inactivation of either the N- or C-domain of ACE were generated, and the C-domain was demonstrated to be the main site of angiotensin I cleavage (18, 22), which is consistent with our *in vitro* finding. However, the role of the N-domain of ACE toward Aβ42 to Aβ40 conversion *in vivo* needs to be addressed.

It has been previously reported that testicular ACE, the C-domain isoform of ACE, without *N*-linked glycosylation has no enzyme activity and was rapidly degraded (19). We confirmed that deglycosylation of human kidney ACE abolished its angiotensin-converting activity, whereas the endopeptidase activity for degrading itself and Aβ42 was not affected. Moreover, the N-domain-specific Aβ42-to-Aβ40-converting activity was abolished by the deglycosylation, indicating that the *N*-linked glycosylation is also essential for maintaining the N-domain-specific enzymatic activity of ACE. Deglycosylated ACE was retained as an intact protein 30 min after deglycosylation. ACE activity and Aβ42-to-Aβ40-converting activity were clearly detected in non-deglycosylated ACE within 30 min (Fig. 4, *B* and *C*). Thus, the loss of ACE activity and Aβ42-to-Aβ40-converting activity of deglycosylated ACE may not result from its self-degradation, but likely result from the deglycosylation. These results suggest that *N*-linked glycosylation is required to maintain the ACE structure and its dipeptidyl carboxypeptidase activity in both N- and C-domains. Presenilins have been shown to be involved in the maturation of membrane proteins, whether presenilin mutants in familial AD affect ACE glycosylation and its Aβ42-to-Aβ40-converting activity need to be clarified in future (23). Finally, we showed that ACE inhibitors inhibited the N-domain-specific Aβ42-to-Aβ40-converting activity each with a different IC_{50}. Among the examined ACE inhibitors, enalaprilat has the strongest inhibitory effect on Aβ42-to-Aβ40-converting activity. This result may provide a mechanism underlying the finding that non-centrally active ACE inhibitors, such as enalapril, are associated with a greater risk of incident dementia (24). In

our previous *in vivo* study, captopril treatment enhanced predominantly brain Aβ42 deposition in 17-month-old amyloid precursor protein (APP) transgenic mice and led to a tendency of increased brain Aβ42/40 ratio (15). Taking the anti-amyloid and antioxidant effects of Aβ40 into account, our findings suggest that ACE inhibitors could be designed specifically to target the C-domain of ACE without inhibiting its N-domain-specific Aβ42-to-Aβ40-converting activity.

Acknowledgments—We thank Dr. Dennis J. Selkoe for providing wtACE, E362D, E960D, and E362/960D plasmids and thank Dr. Paul Langman for English correction.

REFERENCES

1. Kehoe, P. G., and Wilcock, G. K. (2007) *Lancet Neurol.* **6,** 373–378
2. Zou, K., and Michikawa, M. (2008) *Rev. Neurosci.* **19,** 203–212
3. Lehmann, D. J., Cortina-Borja, M., Warden, D. R., Smith, A. D., Sleegers, K., Prince, J. A., van Duijn, C. M., and Kehoe, P. G. (2005) *Am. J. Epidemiol.* **162,** 305–317
4. Kehoe, P. G., Russ, C., Mcllory, S., Williams, H., Holmans, P., Holmes, C., Liolitsa, D., Vahidassr, D., Powell, J., McGleenon, B., Liddell, M., Plomin, R., Dynan, K., Williams, N., Neal, J., Cairns, N. J., Wilcock, G., Passmore, P., Lovestone, S., Williams, J., and Owen, M. J. (1999) *Nat. Genet.* **21,** 71–72
5. Elkins, J. S., Douglas, V. C., and Johnston, S. C. (2004) *Neurology* **62,** 363–368
6. Skoog, I., Lernfelt, B., Landahl, S., Palmertz, B., Andreasson, L. A., Nilsson, L., Persson, G., Odén, A., and Svanborg, A. (1996) *Lancet* **347,** 1141–1145
7. Khachaturian, A. S., Zandi, P. P., Lyketsos, C. G., Hayden, K. M., Skoog, I., Norton, M. C., Tschanz, J. T., Mayer, L. S., Welsh-Bohmer, K. A., and Breitner, J. C. (2006) *Arch. Neurol.* **63,** 686–692
8. Hu, J., Igarashi, A., Kamata, M., and Nakagawa, H. (2001) *J. Biol. Chem.* **276,** 47863–47868
9. Hemming, M. L., and Selkoe, D. J. (2005) *J. Biol. Chem.* **280,** 37644–37650
10. Mucke, L., Masliah, E., Yu, G. Q., Mallory, M., Rockenstein, E. M., Tatsuno, G., Hu, K., Kholodenko, D., Johnson-Wood, K., and McConlogue, L. (2000) *J. Neurosci.* **20,** 4050–4058
11. McGowan, E., Pickford, F., Kim, J., Onstead, L., Eriksen, J., Yu, C., Skipper, L., Murphy, M. P., Beard, J., Das, P., Jansen, K., Delucia, M., Lin, W. L., Dolios, G., Wang, R., Eckman, C. B., Dickson, D. W., Hutton, M., Hardy, J., and Golde, T. (2005) *Neuron* **47,** 191–199
12. Zou, K., Gong, J. S., Yanagisawa, K., and Michikawa, M. (2002) *J. Neurosci.* **22,** 4833–4841
13. Zou, K., Kim, D., Kakio, A., Byun, K., Gong, J. S., Kim, J., Kim, M., Sawamura, N., Nishimoto, S., Matsuzaki, K., Lee, B., Yanagisawa, K., and Michikawa, M. (2003) *J. Neurochem.* **87,** 609–619
14. Kim, J., Onstead, L., Randle, S., Price, R., Smithson, L., Zwizinski, C., Dickson, D. W., Golde, T., and McGowan, E. (2007) *J. Neurosci.* **27,** 627–633
15. Zou, K., Yamaguchi, H., Akatsu, H., Sakamoto, T., Ko, M., Mizoguchi, K., Gong, J. S., Yu, W., Yamamoto, T., Kosaka, K., Yanagisawa, K., and Michikawa, M. (2007) *J. Neurosci.* **27,** 8628–8635
16. Turner, A. J., and Hooper, N. M. (2002) *Trends Pharmacol. Sci.* **23,** 177–183
17. Rousseau, A., Michaud, A., Chauvet, M. T., Lenfant, M., and Corvol, P. (1995) *J. Biol. Chem.* **270,** 3656–3661
18. Fuchs, S., Xiao, H. D., Hubert, C., Michaud, A., Campbell, D. J., Adams, J. W., Capecchi, M. R., Corvol, P., and Bernstein, K. E. (2008) *Hypertension* **51,** 267–274
19. Sadhukhan, R., and Sen, I. (1996) *J. Biol. Chem.* **271,** 6429–6434
20. Oba, R., Igarashi, A., Kamata, M., Nagata, K., Takano, S., and Nakagawa, H. (2005) *Eur. J. Neurosci.* **21,** 733–740
21. Soubrier, F., Alhenc-Gelas, F., Hubert, C., Allegrini, J., John, M., Tregear, G., and Corvol, P. (1988) *Proc. Natl. Acad. Sci. U.S.A.* **85,** 9386–9390
22. Fuchs, S., Xiao, H. D., Cole, J. M., Adams, J. W., Frenzel, K., Michaud, A., Zhao, H., Keshelava, G., Capecchi, M. R., Corvol, P., and Bernstein, K. E. (2004) *J. Biol. Chem.* **279,** 15946–15953
23. Zou, K., Hosono, T., Nakamura, T., Shiraishi, H., Maeda, T., Komano, H., Yanagisawa, K., and Michikawa, M. (2008) *Biochemistry* **47,** 3370–3378
24. Sink, K. M., Leng, X., Williamson, J., Kritchevsky, S. B., Yaffe, K., Kuller, L., Yasar, S., Atkinson, H., Robbins, M., Psaty, B., and Goff, D. C., Jr. (2009) *Arch. Intern. Med.* **169,** 1195–1202

Journal of Neuroscience Research 87:2498–2508 (2009)

Mechanism Underlying Apolipoprotein E (ApoE) Isoform-dependent Lipid Efflux From Neural Cells in Culture

Hirohisa Minagawa,[1] Jiang-Sheng Gong,[1] Cha-Gyun Jung,[1] Atsushi Watanabe,[2] Sissel Lund-Katz,[3] Michael C. Phillips,[3] Hiroyuki Saito,[4] and Makoto Michikawa[1]*

[1]Department of Alzheimer's Disease Research, National Institute for Longevity Sciences, National Center for Geriatrics and Gerontology, Aichi, Japan
[2]Department of Vascular Dementia, National Institute for Longevity Sciences, National Center for Geriatrics and Gerontology, Aichi, Japan
[3]Lipid Research Group, Children's Hospital of Philadelphia, University of Pennsylvania School of Medicine, Philadelphia, Pennsylvania
[4]Department of Biophysical Chemistry, Kobe Pharmaceutical University, Kobe, Japan

We determined the molecular mechanisms underlying apolipoprotein E (ApoE)-isoform-dependent lipid efflux from neurons and ApoE-deficient astrocytes in culture. The ability of ApoE3 to induce lipid efflux was 2.5- to 3.9-fold greater than ApoE4. To explore the contributions of the amino- and carboxyl-terminal tertiary structure domains of ApoE to cellular lipid efflux, each domain was studied separately. The amino-terminal fragment of ApoE3 (22-kDa-ApoE3) induced lipid efflux greater than 22-kDa-ApoE4, whereas the common carboxyl-terminal fragment of ApoE induced very low levels of lipid efflux. Addition of segments of the carboxyl-terminal domain to 22-kDa-ApoE3 additively induced lipid efflux in a length-dependent manner; in contrast, this effect did not occur with ApoE4. This observation, coupled with the fact that introduction of the E255A mutation (which disrupts domain–domain interaction) into ApoE4 increases lipid efflux, indicates that interaction between the amino- and carboxyl-terminal domains in ApoE4 reduces the ability of this isoform to mediate lipid efflux from neural cells. Dimeric 22-kDa or intact ApoE3 induced higher lipid efflux than monomeric 22-kDa or intact ApoE3, respectively, indicating that dimerization of ApoE3 enhances the ability to release lipids. The adenosine triphosphate–binding cassette protein A1 (ABCA1) is involved in ApoE-induced lipid efflux. In conclusion, there are two major factors, intramolecular domain interaction and intermolecular dimerization, that cause ApoE-isoform-dependent lipid efflux from neural cells in culture.

Key words: Alzheimer's disease; apolipoprotein E; high-density lipoprotein (HDL); neurons; astrocyte

The lipoprotein found in the central nervous system (CNS) is the high-density lipoprotein (HDL), and apolipoprotein E (ApoE) is one of the major apolipoproteins regulating lipid transport in CNS (Roheim et al., 1979; Pitas et al., 1987b; Weisgraber et al., 1994). Astrocytes and microglia synthesize and secrete ApoE (Boyles et al., 1985; Nakai et al., 1996), which interacts with adenosine triphosphate (ATP)-binding cassette protein A1 (ABCA1) (Krimbou et al., 2004) to remove cholesterol from cells and generate HDL particles in the cerebrospinal fluid and cultured media (Pitas et al., 1987a; Borghini et al., 1995; LaDu et al., 1998).

ApoE-inducible lipid efflux is ApoE-isoform dependent (Michikawa et al., 2000; Gong et al., 2002; Xu et al., 2004), and ApoE3 generates a similar number of HDL particles to but with a smaller number of ApoE molecules than ApoE4 (Gong et al., 2002). HDL synthesis mediated by ApoE contributes to cholesterol release from the cell membrane. On the other hand, HDL associated with ApoE is taken up by cells via ApoE receptors and the cholesterol in HDL is used for maintaining cholesterol homeostasis in CNS neurons. Thus, this isoform-specific action of ApoE to remove cholesterol and

Contract grant sponsor: Ministry of Health, Labor and Welfare of Japan (Research on Human Genome and Tissue Engineering); Contract grant number: H17-004; Contract grant sponsor: Program for Promotion of Fundamental Studies in Health of the National Institute of Biomedical Innovation (NIBIO); Contract grant sponsor: Japan Society for the Promotion of Science (JSPS); Contract grant sponsor: Naito Foundation; Contract grant sponsor: Grant-in-Aid for Scientific Research on Priority Areas—Research on Pathomechanisms of Brain Disorders, from the Ministry of Education, Culture, Sports, Science and Technology of Japan; Contract grant number: 18023046; Contract grant sponsor: NIH; Contract grant number: HL 56083.

*Correspondence to: Makoto Michikawa, Department of Alzheimer's Disease Research, National Institute for Longevity Sciences (NILS), National Center for Geriatrics and Gerontology (NCGG), 36-3 Gengo, Morioka, Obu, Aichi 474-8522, Japan. E-mail: michi@nils.go.jp

Received 30 September 2008; Revised 27 January 2009; Accepted 8 February 2009

Published online 26 March 2009 in Wiley InterScience (www.interscience.wiley.com). DOI: 10.1002/jnr.22073

generate HDL may be the cause of altered cholesterol metabolism in an Alzheimer's disease (AD) brain (Demeester et al., 2000; Molander-Melin et al., 2005) and may explain how ApoE4 serves as a strong risk factor for AD development (Corder et al., 1993; Strittmatter et al., 1993). However, the molecular mechanism underlying ApoE-isoform-dependent HDL generation remains to be elucidated.

The ApoE molecule has two distinct domains, namely, the 22-kDa amino-terminal (residues 1–191) and 10-kDa carboxyl-terminal domains (residue 218–299), that unfold independently of each other (Wetterau et al., 1988; Morrow et al., 2000). It has been demonstrated that ApoE4 amino- and carboxyl-domain interaction is responsible for the ApoE-isoform dependent association with lipid particles (Weisgraber, 1990; Dong and Weisgraber, 1996; Saito et al., 2003). The domain interaction in ApoE4 under physiological conditions has also been confirmed at the cellular level (Xu et al., 2004) and in vivo (Raffai et al., 2001; Ramaswamy et al., 2005), suggesting that the presence or absence of the domain interaction can explain ApoE-isoform dependent lipid efflux. In addition, there are ApoE-isoform dependent differences in the structure and stability of the 22-kDa amino-terminal fragment (22-kDa-ApoE), which affect their binding affinities to lipids (Morrow et al., 2000, 2002; Segall et al., 2002; Hatters et al., 2005), suggesting that the 22-kDa-ApoE that lacks the domain interaction may also explain an isoform-dependent lipid efflux.

In this study, we investigated the molecular mechanisms, by which intact ApoE3 has a greater ability to induce cholesterol efflux than intact-ApoE4 by using cultured rat neurons and astrocytes prepared from ApoE knockout mouse brain to exclude the effect of endogenously generated and secreted ApoE. We found that the intramolecular amino- and carboxyl-terminal domain interaction is partially responsible for this ApoE-isoform dependency. To our surprise, 22-kDa-ApoE3 has a greater ability to induce cholesterol efflux than 22-kDa-ApoE4. This is because 22-kDa-ApoE3 forms dimers, whereas 22-kDa-ApoE4 does not. These findings suggest that cholesterol efflux induced by ApoE is regulated by two major factors: the presence or absence of intermolecular dimer formation and the intramolecular domain interaction.

EXPERIMENTAL PROCEDURES

Cell Culture

All experiments were performed in compliance with existing laws and institutional guidelines. Neuron-rich cultures were prepared from rat cerebral cortices as previously described (Michikawa et al., 2001). Cerebral cortices from rat brains were dissected, freed of meninges, and diced into small fragments. Cortical fragments were incubated in 2.5% trypsin and 2 mg/ml DNase I in phosphate-buffered saline (PBS) (8.1 mM Na_2HPO_4, 1.5 mM KH_2PO_4, 137 mM NaCl, and 2.7 mM KCl; pH 7.4) at 37°C for 15 min. The fragments were then dissociated into single cells by pipetting. The dissociated cells were suspended in a feeding medium and plated onto poly-D-lysine-coated 12-well plates at a cell density of 1×10^6/ml in Dulbecco modified Eagle's medium nutrient mixture (DMEM/F-12; 50:50%) containing N_2 supplements plus 7.5% bovine albumin fraction V.

Highly astrocyte-rich cultures were prepared according to a previously described method (Michikawa et al., 2001). In brief, brains of postnatal day 2 ApoE knockout mice were removed under anesthesia. The cerebral cortices from the mouse brains were dissected, freed of meninges, and diced into small fragments. Cortical fragments were incubated in 0.25% trypsin and 2 mg/ml DNase I in PBS (8.1 mM Na_2HPO_4, 1.5 mM KH_2PO_4, 137 mM NaCl and 2.7 mM KCl; pH 7.4) at 37°C for 15 min. The fragments were then dissociated into single cells by pipetting. The dissociated cells were seeded in 75-cm^2 dishes at a cell density of 1×10^7 in DMEM nutrient mixture containing 10% FBS and 1% penicillin/streptomycin solution (Invitrogen Corporation, Carlsbad, CA). After 10 days of incubation in vitro, astrocytes in the monolayer were trypsinized (0.1%) and reseeded onto twelve-well dishes. The astrocyte-rich cultures were maintained in DMEM containing 10% FBS until use.

ApoE Preparation

The full-length human ApoE3 and ApoE4 and their 22- and 10-kDa fragments were expressed and purified as described (Saito et al., 2001). The cDNA for full-length human ApoE3 and ApoE4, the 22-kDa fragments, or the 10-kDa fragment were ligated into a thioredoxin fusion expression vector pET32a and transformed into the *Escherichia coli* strain BL21 star (DE3). The transformed *E. coli* were cultured in LB medium at 37°C, and thioredoxin-ApoE expression was induced with isopropyl-β-D-galactopyranoside for 3 hr. After the bacterial pellet was sonicated and the lysate was centrifuged to remove debris, the fusion protein was cleaved with thrombin to remove thioredoxin from full-length ApoE3, ApoE4 or the 22- or 10-kDa fragment. For the full-length ApoE3 and ApoE4, the fusion protein was complexed with DMPC before it was cleaved with thrombin to protect the protease susceptible internal hinge region. After inactivation of the thrombin with β-mercaptoethanol, the mixture was lyophilized and delipidated, and the ApoE pellet was dissolved in 6 M guanidine–HCl, pH 7.4, containing 1% β-mercaptoethanol. The ApoE was isolated by gel filtration chromatography on a Sephacryl S-300 column. For further purification (>95%), the proteins were subjected to gel filtration with a Superdex 75 column or anion exchange chromatography with a HiTrap Q column

When we used ApoE and ApoE fragments, the recombinant ApoEs were dissolved in 5 M guanidine–HCl. The resulting solutions were dialyzed against PBS at 4°C for 16 hr. Each ApoE level was determined with a BCA protein assay kit (Pierce, Rockford, IL).

Determination of Levels of Cholesterol and Phosphatidylcholine (PC) Released From Neurons and Astrocytes Labeled With [^{14}C]acetate

Astrocytes plated in twelve-well dishes were cultured in DMEM containing 10% FBS and 1% penicillin/streptomycin

solution for 72 hr. The cultures were then treated with 37 kBq/ml [^{14}C]acetate (Moravek Biochemicals Inc., Brea, CA) for 48 hr. The astrocytes were washed in DMEM two times and treated with 0.3 μM ApoE in DMEM for 24 hr. To analyze dose-dependent effects, the astrocytes were treated with 0.03 μM, 0.1 μM, 0.3 μM and 1.0 μM ApoE; to analyze time-dependent effects, the astrocytes were treated and maintained for 8, 24 and 48 hr. The culture medium was quickly removed and the astrocytes were dried at room temperature. 1.0 ml of the conditioned culture medium was extracted with 4.0 ml of hexane/isopropyl alcohol (3:2 v/v). For the extraction of intracellular lipids, dried astrocytes were incubated in hexane/isopropyl alcohol (3:2 v/v) for 1 hr at room temperature. The solvent from each plate was removed and dried under N_2 gas. The organic phase was redissolved in 200 μl of hexane/isopropyl alcohol (3:2 v/v), and 10 μl of each sample was spotted on activated-silica-gel high- performance thin layer chromatography plates (Merck); the lipids were separated by sequential one-dimensional chromatography by using chloroform/methanol/acetic acid/water (25:15:4:2, v/v), followed by another run in hexane/diethyl ether/acetic acid (80:30:1). [^{14}C]Cholesterol and [^{14}C]PC were used as standards. The chromatography plates were exposed to radiosensitive films, and each lipid was visualized and quantified with BAS2500 (Fuji Film, Tokyo, Japan). The levels of [^{14}C]cholesterol and [^{14}C]PC efflux were calculated by the following formula: % efflux = media × 100/(media + cell).

Dimerization of 22-kDa-ApoE3

The pure 22-kD-ApoE3 was obtained by reduction with 10 mM dithiothreitol (DTT) in 5 M guanidine–HCl buffer. The dimer was formed by incubation of the monomer in oxygenated 5 M guanidine–HCl at 10 mg/ml for 2 weeks at 4°C. Residual monomer was removed by passage of the protein solution through a thiopropyl Sepharose 6B column (GE Healthcare, Piscataway, NJ) according to the manufacturer's instructions.

Dimerization of Intact ApoE3

The ApoE3 (1 mg/ml in 6 M urea, and 10 mM Tris-HCl) used was a mixture of monomeric and dimeric ApoEs. The mixture was reduced to generate monomeric ApoE3 by adding 10 mM DTT, incubated at 4°C for 16 hr, dialyzed against 6 M urea in 10 mM Tris-HCl solution, and oxidized by stirring at 4°C for 3 days. Then it was loaded onto a 2-ml-bed-volume prepacked 6% cross-linked beaded agarose gel column with a SulfoLink kit (Pierce, Rockford, IL) and equilibrated with PBS. Dimeric ApoE3 was eluted with PBS.

Western Blot Analysis of Dimeric 22-kDa-ApoE3 by Nonreducing Gel Electrophoresis

To determine the ratio of dimeric 22-kDa-ApoE3 in the solution, Western blot analysis was performed under nonreducing conditions. Dimeric 22-kDa-ApoE3 was mixed with the same volume of a 2× nonreducing Laemmli buffer consisting of 100 mM Tris-HCl (pH 7.4), 10% glycerol, 4% SDS, and 0.01% bromophenol blue, and analyzed by 4–12% Tris/Tricine sodium dodecyl sulfate–polyacrylamide gel electrophoresis (SDS-PAGE) (Daiichi Pure Chemicals Co., Tokyo, Japan). The separated proteins were transferred onto Immobilon membranes with a semidry electrophoretic transfer apparatus (Nihon Eido, Tokyo, Japan) with a transfer buffer (0.1 M Tris-HCl (pH 7.4), 0.192 M glycine, and 20% methanol). The blots were probed for 16 hr at 4°C with a goat anti-ApoE polyclonal antibody, AB947 (1:2,000; Chemicon, Temecula, CA). Band detection was carried out with an ECL kit (GE Healthcare UK Ltd., England).

Purification and Carboxamidomethylation of Recombinant Intact ApoE3

ApoE3 was dissolved in 5 M guanidine–HCl, 10 mM EDTA, 200 mM Tris-HCl (pH8.5), and half of each protein solution was reduced with 10 mM DTT at room temperature for 2 hr and alkylated with 40 mM iodoacetamide in the dark at room temperature for 30 min, as described previously (Franceschini et al., 1990). All the proteins were then purified on an Aquapore RP300 column (2.1 × 30 mm; Applied Biosystems; Foster City, CA) by reverse-phase high-performance liquid chromatography (HPLC; model 1100 Series; Agilent Technology, Waldbronn, Germany) with a linear gradient of 36–52% acetonitrile in 0.1% trifluoroacetic acid for 16 min and a linear gradient of 52–76% acetonitrile in 0.1% trifluoroacetic acid for 1 min at a flow rate of 0.2 ml/min. The HPLC-purified ApoE3 was lyophilized and kept at −30°C until use.

Effect of 22-hydroxycholesterol and Glyburide on 22-kDa-ApoEs-induced Lipid Efflux

Neuron cultures were prepared, maintained, and labeled with [^{14}C]acetate, and exposed to 22-kDa-ApoE3 dimer or 22-kDa-ApoE3 monomer at a concentration of 0.3 μM in the presence of 22-hydroxycholesterol (10 μM) or glyburide (500 μM) for 24 hr. The lipids released into the media and the lipids retained in the cells were then determined. The expression level of ABCA1 in the cultures for each treatment was determined by Western blot analysis with anti-ABCA1 antibody (Santa Cruz, Santa Cruz, CA) used as a primary antibody.

RNA Interference

To knock down the endogenous ABCA1, primary cultured neurons and astrocytes were transiently transfected with 50 nM of the synthesized small interfering RNAs (siRNAs) targeting ABCA1 or with the Stealth siRNA negative control (Invitrogen) with Lipofectamine RNAiMAX (Invitrogen) according to the manufacturer's protocol. ABCA1 siRNA sequences is as follows: ABCA1-siRNA sense (5′-CA GGAUUUCCUGGUGGACAAUGAAA-3′) and antisense (5′-UUUCAUUGUCCACCAGGAAAUCCUG-3′).

Statistical Analysis

StatView computer software (Windows) was used for statistical analysis. The statistical significance of differences between samples was evaluated by multiple pairwise comparisons among the sets of data by ANOVA and the Bonferroni *t*-test.

RESULTS

Primary-cultured neurons and astrocytes were prepared and the levels of cholesterol and PC efflux were determined as described in Experimental Procedures. The levels of cholesterol and PC released from neurons in the medium treated with ApoE3 at 0.3 μM were significantly greater than those in the medium treated with ApoE4 (Fig. 1A). The level of cholesterol released by ApoE4 was 25% of that released by ApoE3. The reduced levels of cholesterol and PC efflux induced by ApoE4 increased significantly, although not to the level induced by ApoE3, when the neurons were incubated with the apoE4 (E255A) mutant (mt-ApoE4), which has altered amino- and carboxyl-terminal domain interaction because there is no electrostatic interaction between Arg61 and Glu255 (Dong and Weisgraber, 1996) (Fig. 1A). The partial recovery in the level of lipid efflux induced by mt-ApoE4 suggests that mechanisms other than the domain interaction are involved in ApoE-isoform-dependent lipid efflux from neurons in culture. Similar results were observed with cultured astrocytes. The levels of cholesterol and PC released from astrocytes in the medium treated with ApoE3 at 0.3 μM were significantly greater than those in the medium treated with ApoE4 (Fig. 1B). The levels of cholesterol and PC efflux induced by ApoE4 increased significantly, although not to the level induced by ApoE3, when the astrocytes were incubated with mt-ApoE4 (Fig. 1B).

We also examined the effect of the ApoE fragments on lipid efflux from cultured neurons and astrocytes to determine which part of the ApoE molecule is responsible for lipid efflux and ApoE isoform dependency. Interestingly, the 22-kDa fragment of ApoE (22-kDa-ApoE) induced cholesterol and PC efflux, which were ApoE-isoform-dependent (Fig. 1A,B). Unexpectedly, the carboxyl-terminal 10-kDa-ApoE and 12-kDa-ApoE, both of which contain the lipid binding site, have a very weak ability to release lipids (Fig. 1A,B).

Figure 2A shows the time-dependent cholesterol and PC efflux from neurons induced by 22-kDa-ApoE3 and 22-kDa-ApoE4 at 0.3 μM. The level of lipids released by 22-kDa-ApoE3 was significantly greater than that by 22-kDa-ApoE4 at time points of 24 and 48 hr (Fig. 2B). The level of cholesterol and PC efflux induced by 22-kDa-ApoE 24 hr after the treatment increased in an ApoE-concentration-dependent manner (Fig. 2B). The levels of cholesterol and PC efflux induced by 22-kDa-ApoE3 were greater than those released by 22-kDa-ApoE4 at 0.3 and 1.0 μM (Fig. 2B). Time- and ApoE-dose-dependent lipid efflux was also examined with ApoE-deficient astrocyte cultures, and the similar results were observed (Fig. 2C,D).

The results in Figures 1 and 2 indicate that the amino-terminal domain, the 22-kDa fragment, induces lipid efflux in an ApoE-isoform dependent manner, whereas the carboxyl-terminal domain, the 10-kDa fragment, has a very weak ability to induce lipid efflux from cultured astrocytes. These results raise the question of how the amino-terminal and carboxyl-terminal domains

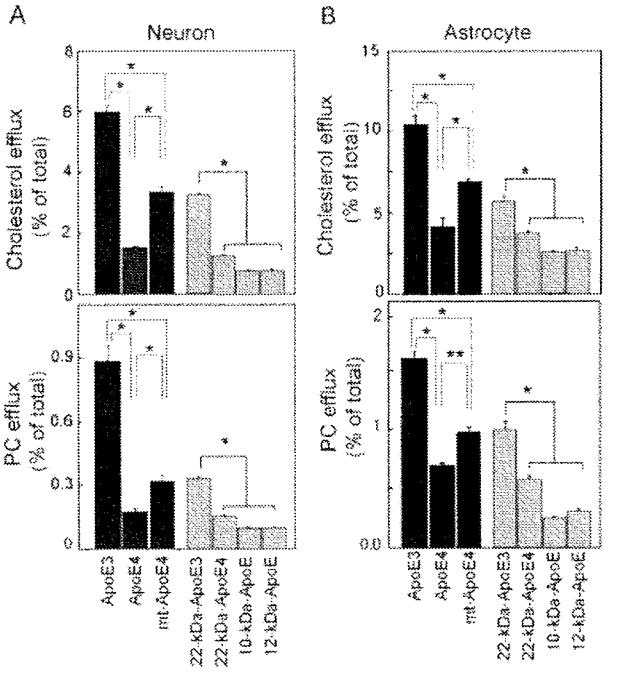

Fig. 1. Cholesterol and PC efflux from cultured neurons and astrocytes induced by ApoEs. Neurons and astrocytes were prepared as described in Experimental Procedures. The neurons (**A**) and astrocytes (**B**) were cultured for 72 hr, labeled with [^{14}C]acetate for 48 hr, and exposed to intact, lipid-free, ApoE3(residues 1–299), ApoE4, mt-ApoE4(E255A), 22-kDa-ApoE3 (residues 1–191), 22-kDa-ApoE4, 10-kDa-ApoE (residues 218–299), and 12-kDa-ApoE (residues 192–299) fragments at 0.3 μM for 24 hr. The lipids released into the media and the lipids retained in the cells were extracted and analyzed as described in Experimental Procedures. The percentages of released cholesterol and PC levels over the total levels were calculated. Data are means ± SE of four samples. $*P < 0.0001$ and $**P < 0.0005$. Three independent experiments showed similar results. The basal value of cholesterol and PC efflux in the absence of ApoEs are 1.0 ± 0.1 (%) and 0.4 ± 0.1 (%), respectively.

contribute to lipid efflux induced by intact ApoE in an ApoE-isoform-dependent manner. To answer this question, we examined whether the carboxyl-terminal domain of ApoE modifies lipid efflux caused by 22-kDa-ApoE. The ApoEs used were 22-kDa-ApoE (amino acids, 1–191) and 22-kDa-ApoE with carboxyl-terminal fragment of various lengths, that is, ApoEs harboring amino acids 1–250, 1–260, 1–272, and 1–299 (intact ApoE). As shown in Figure 3A, cholesterol and PC efflux induced by ApoE3 species from cultured neurons depended on the carboxyl-terminal fragment length; that is, ApoE3 variants with a longer carboxyl-terminal region induced progressively more lipid efflux. However, such is not the case for ApoE4. The addition of a carboxyl-terminal region ending at amino acid 250 increased the level of lipid efflux significantly more than 22-kDa-ApoE4; however, 22-kDa-ApoE4 with a car-

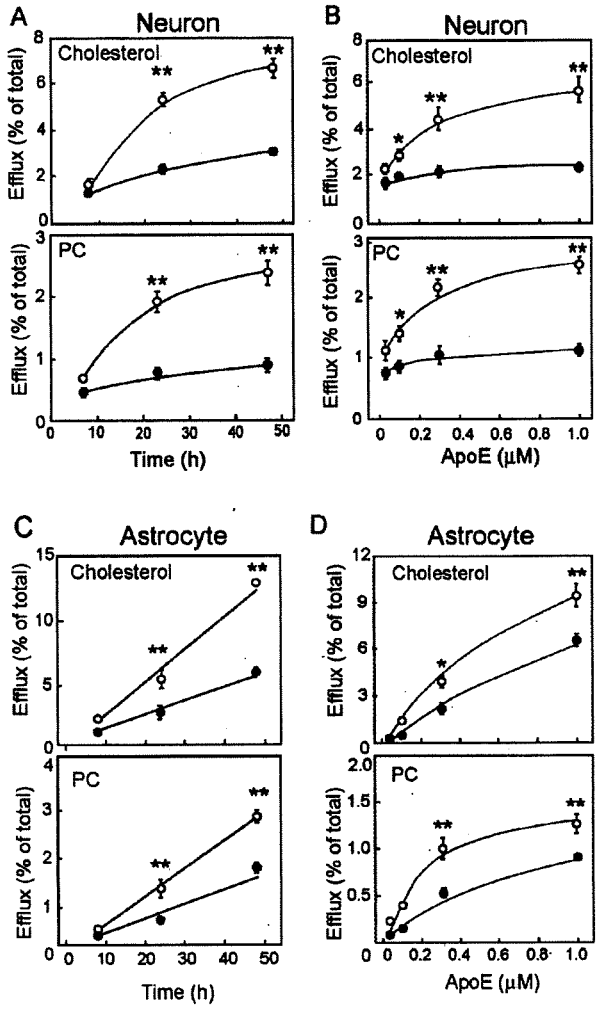

Fig. 2. Time- and dose-dependent lipid efflux mediated by 22-kDa-ApoE fragment. Cultured neurons and astrocytes were prepared, maintained, and labeled with [^{14}C]acetate as described in the legend for Fig. 1. For determination of the time-dependent lipid release from neurons (**A**) and astrocytes (**C**), each culture was exposed to 22-kDa-ApoE3 (open circle) and 22-kDa-ApoE4 (closed circle) at 0.3 μM for 8, 24, and 48 hr. For determination of the dose-dependent lipid release from neurons (**B**) and astrocytes (**D**), each culture was exposed to 22-kDa-ApoE3 (open circle) and 22-kDa-ApoE4 (closed circle) at varying concentrations for 24 hr. The lipids released into the media and the lipids retained in the cells were determined as described in Experimental Procedures. (**B**) For determination of Data are means ± SE of four samples. $*P < 0.05$ and $**P < 0.0005$ vs. 22-kDa-ApoE4 at each time point. The basal value of cholesterol and PC efflux in the absence of ApoEs are less than 0.8 ± 0.05 and 0.66 ± 0.11, respectively (**A**), and 0.59 ± 0.04 and 0.39 ± 0.04, respectively (**B**).

boxyl- terminal region longer than 250 amino acid residues lost the additional effect of the carboxyl-terminal region on lipid efflux. The levels of cholesterol and PC efflux induced by mt-ApoE4 recovered significantly but partially, and they did not reach those induced by intact ApoE3, similar to the result shown in Figure 1. Similar results were observed when ApoE-deficient astrocyte cultures were used (Fig. 3B).

The above results suggest that the amino-terminal domain basically determines the ability of ApoE to induce lipid efflux and that the carboxyl-terminal region enhances this ability when the amino and carboxyl domain interaction is absent. Because the absence or presence of cysteine at position 112 in the amino-terminal domain differentiates ApoE3 from ApoE4, it is possible to assume that this one-amino-acid difference results in intra- or intermolecular structural differences leading to the domain interaction or dimerization, respectively. Thus, we examined the effect of the dimer formation of 22-kDa-ApoE3 through disulfide bonds on lipid efflux from neurons and cultured astrocytes. To determine directly whether the dimeric form of 22-kDa-ApoE3 induces greater lipid efflux from astrocytes than the monomeric form, the pure dimeric form of 22-kDa-ApoE3 was prepared as described in Experimental Procedures. To obtain a solution containing the pure monomeric form of 22-kDa-ApoE3, 22-kDa-ApoE3 was dissolved in 5 M guanidine–HCl and 10 mM DTT. The resulting solutions were dialyzed against PBS at 4°C for 16 hr and used for the experiment. The purity of dimer and monomer in each sample was confirmed by Western blot analysis (Fig. 4). We also used 22-kDa-ApoE4 as monomeric ApoE molecule for the experiment that used astrocyte cultures because 22-kDa-ApoE4 contains no cysteine and it remains monomeric (Fig. 4B). The results demonstrated that dimeric form of 22-kDa-ApoE3 induced greater lipid efflux than the monomeric form of 22-kDa-ApoE3 and 22-kDa-ApoE4 in both neuron and astrocyte cultures (Fig. 4). Importantly, regardless of ApoE isoform, monomeric 22-kDa-ApoEs induces similar level of lipid efflux (Fig. 4B).

To determine whether such is the case for intact ApoEs, we examined the effect of the dimer formation of ApoE3 through disulfide bonds on lipid efflux from cultured neurons. We obtained dimer-enriched ApoE3 solutions by using a SulfoLink kit as described under Experimental Procedures. We also used ApoE3 solutions prepared without dimer enrichment, containing monomers and relatively few dimers. We also examined the effect of monomeric ApoEs, namely ApoE4 and ApoE3, whose cysteine was modified by carboxamidomethylation (ApoE3-CM). The levels of cholesterol and PC released from neurons treated with dimer-enriched ApoE3 were 2.9- and 7.6-fold greater than those released from neurons treated with ApoE3 and ApoE3 monomers (ApoE3-CM), respectively (Fig. 5). The effects of ApoE3-CM and ApoE4 on lipid efflux were similar. A Western blot analysis of each sample was performed and results show that the samples contained different amounts of dimers (Fig. 5B). The percentages of ApoE3 dimers as calculated by a densitometric analysis of the bands on the Western blot films were 64.5%,

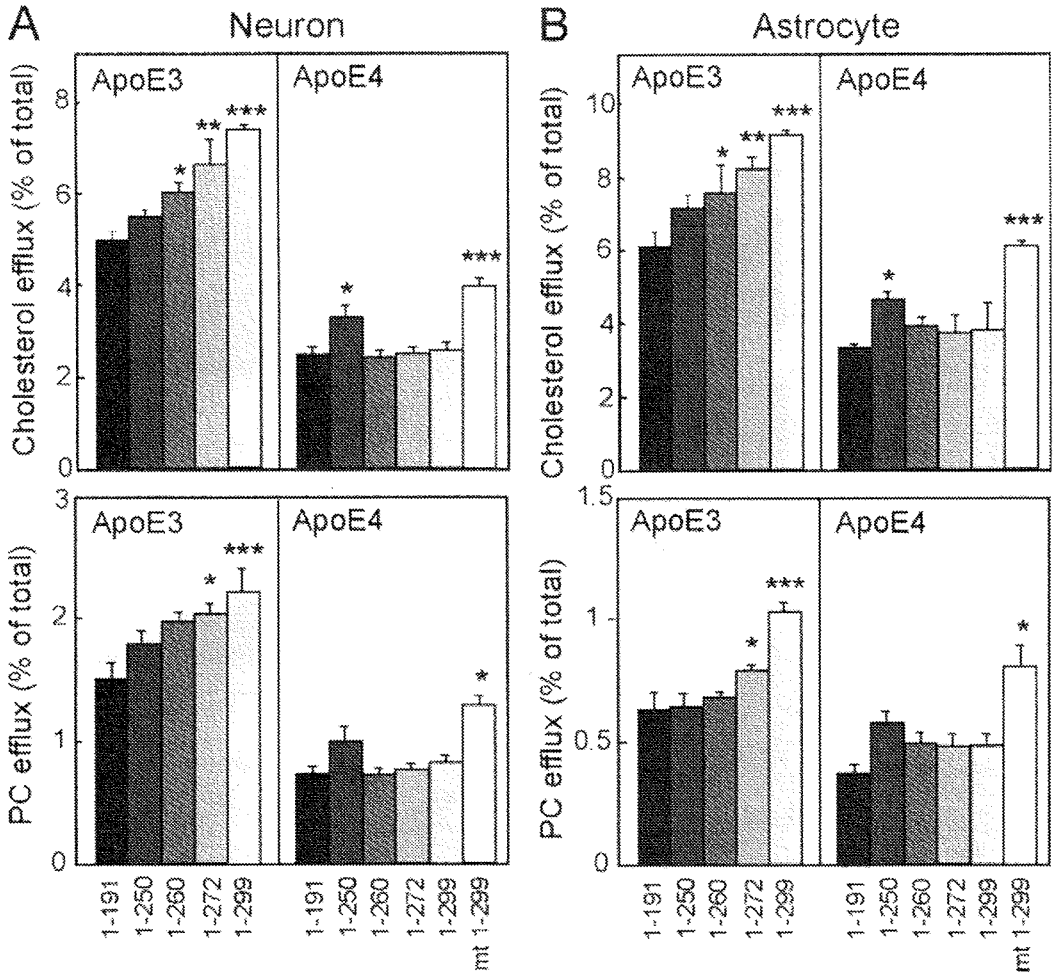

Fig. 3. Cooperative effects of amino- and carboxyl-terminal regions of ApoE on lipid efflux. Neurons and astrocytes were prepared, maintained, and labeled with [^{14}C]acetate as described in the legend for Fig. 1. The neurons (**A**) and astrocytes (**B**) were then exposed to ApoE with carboxyl-terminal regions of various lengths including 1–250, 1–260, 1–272, and 1–299 (full-length ApoE) at 0.3 μM for 24 hr, and the lipids released into the media and the lipids retained in the cells were determined as described in Experimental Procedures. For comparison, the effect of mt-ApoE4 was also determined. Data are means ± SE of four samples. $*P < 0.05$, $**P < 0.005$, and $***P < 0.0001$ vs. 22-kDa-ApoE (1–191). The basal value of cholesterol and PC efflux in the absence of ApoEs are less than 0.8 ± 0.05 and 0.66 ± 0.11, respectively (A, B).

36.9%, 1.8%, and 1.4% in the dimer-enriched ApoE3, non-dimer-enriched ApoE3, ApoE3-CM, and ApoE4 samples, respectively.

Next we determined the involvement of ABCA1 in 22-kDa-ApoEs-induced lipid efflux. The neuron cultures were treated with 22-kDa-ApoE3 dimers, 22-kDa-ApoE3 monomers, or 22-kDa-ApoE4 (monomers) concomitant with 10 μM of 22-hydroxycholesterol, an LXR ligand to up-regulate *ABCA1* gene expression (Wang et al., 2001), and the cultures were maintained for 24 hr. After 24 hr incubation, the level of lipids released into the medium was determined. The ABCA1 expression level was enhanced when the neurons were treated with 22-hydroxycholesterol (Fig. 6A). The levels of lipids released by these ApoE fragments were significantly enhanced when the cultures were concomitantly treated with 22-hydroxycholesterol (Fig. 6B). These results suggest that ABCA1 plays a key role in 22-kDa-ApoEs-mediated lipid efflux in neurons. In support of this notion, we have observed that the treatment of neurons with glyburide, an inhibitor of the ABCA1 transporter, resulted in decreased levels of 22-kDa-ApoE3-mediated cholesterol efflux (Fig. 6C). We further examined the effect of ABCA1 knockdown on 22-kDa ApoEs-mediated lipid efflux by using specific siRNAs. The knockdown of ABCA1 in neurons significantly reduced lipid efflux induced by 22-kDa-ApoE3 dimers (Fig. 7).

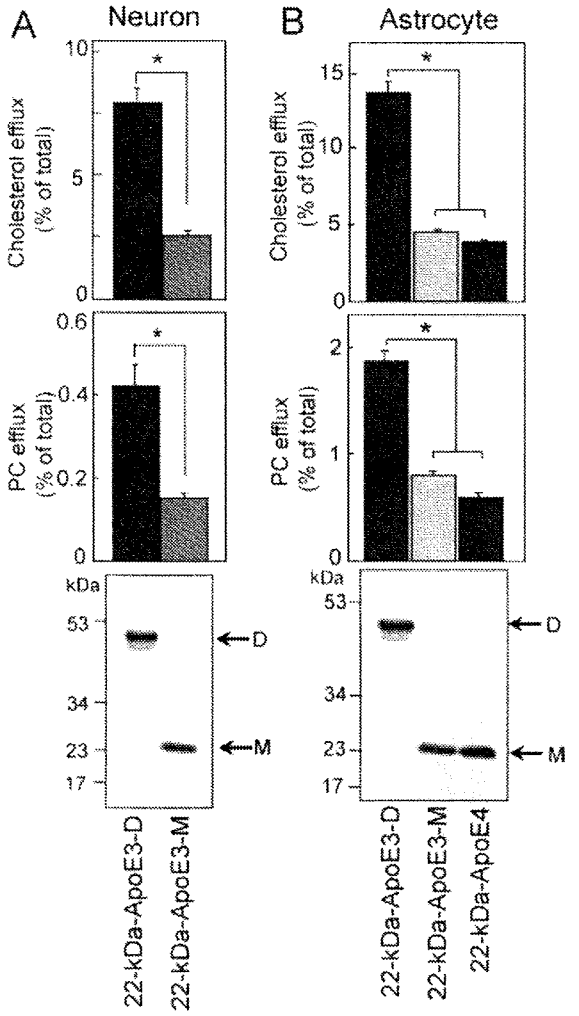

Fig. 4. The ability of 22-kDa-ApoE to induce lipid efflux depends on the ApoE self-association state, i. e., monomer vs dimer. Preparation of 22-kDa-ApoE3 dimer (22-kDa-ApoE3-D), monomer (22-kDa-ApoE3-M), or 22-kDa-ApoE4 monomer was performed as described in Experimental Procedures. **A:** The same amount of 22-kDa-ApoE3-D or 22-kDa-ApoE3-M was subjected to SDS-PAGE under nonreducing conditions, and Western blot analysis was performed with the anti-ApoE antibody AB947. D; dimers, M; monomer. Neuron cultures were prepared, maintained, and labeled with [^{14}C]acetate and exposed to 22-kDa-ApoE3-D or 22-kDa-ApoE3-M at 0.3 μM for 24 hr. The cholesterol and PC efflux by dimeric and monomeric 22-kDa-ApoE3 was determined. **B:** The same amount of 22-kDa-ApoE3 dimers, 22-kDa-ApoE3 monomers, and 22-kDa-ApoE4 monomers was subjected to SDS-PAGE under nonreducing conditions, and Western blot analysis was performed with the anti-ApoE antibody AB947. D; dimers, M; monomer. Astrocyte cultures were prepared, maintained, and labeled with [^{14}C]acetate and exposed to 22-kDa-ApoE3-D, 22-kDa-ApoE3-M, or 22-kDa-ApoE4 monomer at 0.3 μM for 24 hr. The cholesterol and PC efflux by dimeric and monomeric 22-kDa-ApoE3, and monomeric 22-kDa-ApoE4 was determined. Data are means ± SE of four samples. $*P < 0.0001$ vs. 22-kDa-ApoE3. The basal value of cholesterol and PC efflux in the absence of ApoEs are less than 1.41 ± 0.06 and 0.55 ± 0.03, respectively (A, B).

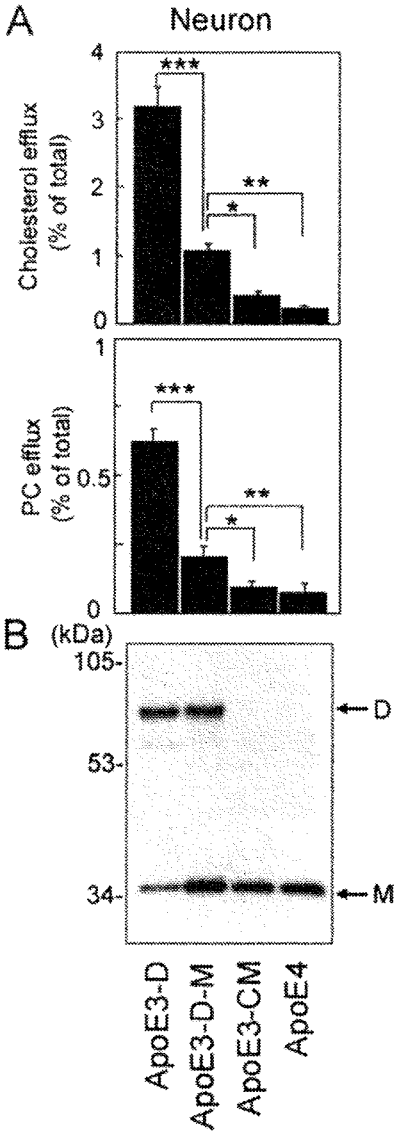

Fig. 5. Effect of intact ApoE dimers on lipid efflux from cultured neurons. A dimer-rich ApoE3 solution was obtained with a column that traps SH residues (monomeric ApoE3s). Carboxamidomethylated ApoE with iodoacetamide was prepared as described in Experimental Procedures. Neuronal cultures were prepared, maintained, and labeled with [^{14}C]acetate and exposed to dimer-enriched ApoE3, ApoE3, ApoE3-CM, and ApoE4 at 0.3 μM for 24 hr. **A:** The levels of cholesterol and PC released into the media and those retained in the cells were determined as described in Experimental Procedures. **B:** To determine the amount of dimers in the samples, Western blot analysis was performed under nonreducing conditions with anti-ApoE antibody AB947 used as the primary antibody. Data are means ± SE of four samples. $*P < 0.01$, $**P < 0.001$, $***P < 0.0001$. The basal value of cholesterol and PC efflux in the absence of ApoEs are 1.54 ± 0.05 and 0.56 ± 0.05, respectively.

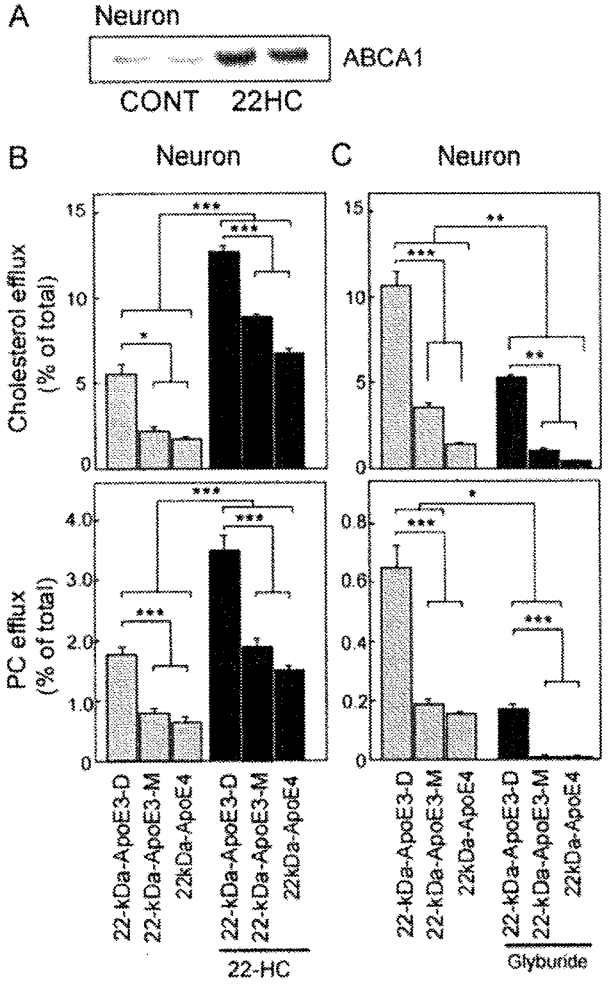

Fig. 6. The effect of 22-hydroxycholesterol and glyburide on 22-kDa-ApoEs-induced lipid efflux. Neuron cultures were prepared, maintained, and labeled with [^{14}C]acetate as described in Fig. 1, and exposed to 22-kDa-ApoE3 dimer (22-kDa-ApoE3-D), 22-kDa-ApoE3 monomer (22-kDa-ApoE3-M), or 22-kDa-ApoE4 at a concentration of 0.3 μM in the presence of 22-hydroxycholesterol (HC) at a concentration of 10 μM for 24 hr. (**A**) The expression level of ABCA1 in the cultures for each treatment was determined by Western blot analysis, and (**B**) the lipids released into the media and the lipids retained in the cells were determined. (**C**) [^{14}C]acetate-labeled neuron cultures were exposed to 22-kDa-ApoE3 dimer (22-kDa-ApoE3-D), 22-kDa-ApoE3 monomer (22-kDa-ApoE3-M), or 22-kDa-ApoE4 at a concentration of 0.3 μM in the presence of glyburide (500 μM) for 24 hr. The lipids released into the media and the lipids retained in the cells were determined. Data are means ± SE of four samples. $*P < 0.05$, $**P < 0.01$, and $***P < 0.0005$. Three independent experiments showed similar results. The basal value of cholesterol and PC efflux in the absence of ApoEs are 5.45 ± 0.51 and 0.58 ± 0.06, respectively.

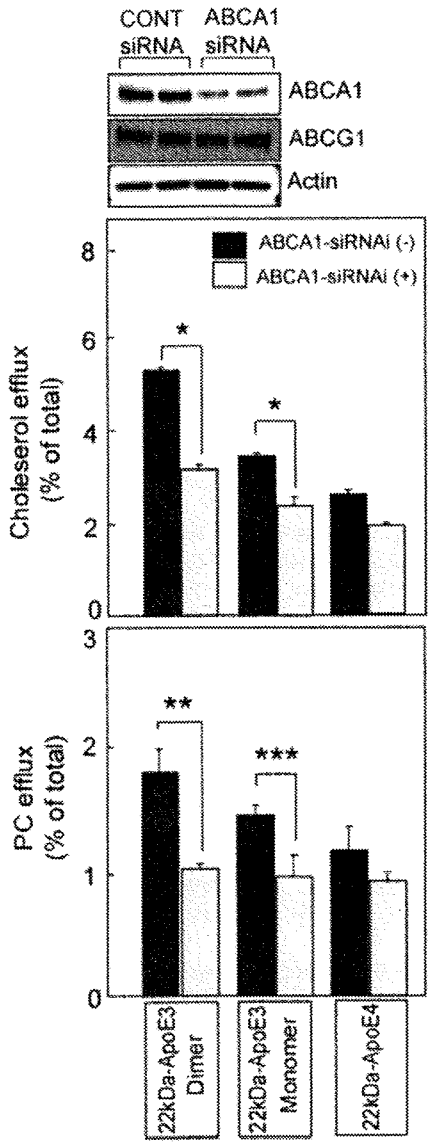

Fig. 7. Lipid efflux by 22-kDa-ApoEs is mediated by ABCA1. The primary neurons, which had been labeled with [^{14}C]acetate and treated with siRNA against ABCA1 for 48 hr, were exposed to 22-kDa-ApoE3 dimer (22-kDa-ApoE3-D) or 22-kDa-ApoE3 monomer (22-kDa-ApoE3-M) at a concentration of 0.3 μM, and maintained for 24 hr. The lipids released into the media and the lipids retained in the cells were then determined as described in Experimental Procedures. Data are means ± SE of four samples. $*P < 0.0001$, $**P < 0.002$, $***P < 0.02$. Three independent experiments showed similar results. The basal value of cholesterol and PC efflux in the absence of ApoEs are 0.89 ± 0.08 and 0.97 ± 0.14, respectively. Those values are 0.84 ± 0.08 and 0.46 ± 0.07 in the siABCA1 experiment.

DISCUSSION

We showed here that lipid efflux induced by ApoE is mainly mediated by the amino-terminal domain of ApoE and modified by the carboxyl-terminal domain. What we found are that the amino-terminal domain of ApoE induces lipid efflux in an isoform-dependent manner and the carboxyl-terminal domain enhances lipid efflux mediated by the amino-terminal domain of ApoE3. In contrast, the carboxyl-terminal domain does not strengthen the lipid efflux mediated by the amino-terminal domain of ApoE4 because of the domain interaction between the amino- and carboxyl-terminal domains. We also found that the lipid efflux induced by these ApoEs is mediated in an ABCA1-dependent manner.

Two of the main findings in this study are that the amino-terminal domain of ApoE, 22-kDa-ApoE, induces lipid efflux and that the extent of lipids released by the amino-terminal domain of ApoE, 22-kDa-ApoE3, is approximately 66% of that induced by intact ApoE3. The carboxyl-terminal domain synergistically and additively modifies lipid efflux mediated by 22-kDa-ApoE3. The additional contribution of the carboxyl-terminal domain is not observed in the case of ApoE4. Basically, 22-kDa-ApoE4 has a very weak ability to induce lipid efflux; moreover, the carboxyl-terminal region of ApoE does not effectively or additively enhance the lipid efflux mediated by 22-kDa-ApoE4. The lack of an additive effect by the carboxyl-terminal region on lipid efflux is likely due to the domain interaction, because an ApoE4 fragment ending at 250 (ApoE1–250) significantly gains in ability to release lipids; however, a carboxyl-terminal region longer than the amino acid 255, glutamate, which interacts with arginine at 61 (called the domain interaction; Dong and Weisgraber, 1996), does not induce any additive effect on lipid efflux induced by 22-kDa-ApoE4.

Another important finding regarding the effect of the domain interaction is that lipid efflux induced by mt-ApoE4 shows only a partial recovery toward the level exhibited by ApoE3. This indicates that the presence or absence of the amino and carboxyl domain interaction cannot completely explain ApoE-isoform-dependent lipid efflux mediated by intact ApoE and that other mechanisms are responsible for such ApoE-isoform dependency. This is supported by the finding of this study that 22-kDa-ApoE, which has no carboxyl-terminal region and thus has no domain interaction, induces lipid release in an ApoE-isoform-dependent manner.

We have already shown that α-helix formation is required for the high-affinity binding of apolipoprotein A-I to lipids (Saito et al., 2004), and that the binding capacity of 22-kDa-ApoE3 is lower than that of 22-kDa-ApoE4 for lipid particles (Saito et al., 2003). On the basis of the facts that the structural stabilities of 22-kDa-ApoE3 and 22-kDa-ApoE4 determine their binding affinity to lipids (Morrow et al., 2002; Segall et al., 2002; Weers et al., 2003) and that 22-kDa-ApoE4 is less stable than 22-kDa-ApoE3 (Morrow et al., 2000), it is reasonable to predict that the level of lipid efflux induced by 22-kDa-ApoE4 would be greater than that induced by 22-kDa-ApoE3. However, our results show the opposite, indicating that ApoE-isoform-dependent cholesterol efflux is unlikely to be explained by a simple theory linking the structural difference between these two fragments with their binding affinity to lipids.

Therefore, the question arises as to what is the mechanism underlying the isoform dependency of 22-kDa-ApoE-induced lipid efflux. It is possible to assume that 22-kDa-ApoE induces lipid efflux, because the 22-kDa domain contains an amphipathic four-helix bundle (Wilson et al., 1991), and it can bind to and reorganize phospholipid vesicles to form discoidal complexes (Lu et al., 2000; Segall et al., 2002). Surprisingly, 22-kDa-ApoE-induced lipid efflux is ApoE-isoform dependent. Such isoform dependency is likely to be caused by the presence or absence of cysteine at residue 112, which may result in intra- or intermolecular structural changes, forming dimers of 22-kDa-ApoE through disulfide bonds. More direct evidence that the dimeric form of 22-kDa-ApoE3 induces greater lipid efflux from cultured neurons and astrocytes than the monomeric form (Fig. 4) supports this idea. Previous reports have demonstrated that cellular cholesterol efflux is induced by many apolipoproteins in their lipid-free form, including ApoA-I, ApoA-II, ApoA-IV, and ApoCIII in addition to ApoE, all of which harbor multiple segments of amphiphilic helices (Segrest et al., 1992); the reaction still occurs with shorter apolipoproteins but to a lesser extent and only at high concentrations (Bielicki et al., 1992). Synthetic amphipathic helical peptides that mimic the physical properties of amphipathic helical segments of apolipoproteins can also induce cholesterol efflux as long as the peptide has at least two such helical segments (Mendez et al., 1994; Yancey et al., 1995). Consistent with these lines of evidence, when human ApoA-II, a disulfide-linked dimer, is reduced to a carboxyamidomethylation monomeric form, the ability of ApoA-II to induce cholesterol efflux is significantly decreased (Hara et al., 1992). In addition, the disulfide- linked homodimer of ApoE3 has been identified not only in cell culture medium (Gong et al., 2002), but also in human plasma (Weisgraber and Shinto, 1991). The mechanism by which the ApoE and ApoA-II dimers gain their functions to release higher amounts of lipids than ApoE and ApoA-II monomers, respectively, remains to be elucidated.

ABCA1 is involved in apolipoprotein-induced lipid efflux, including that mediated by ApoA-I (Brooks-Wilson et al., 1999; Lawn et al., 1999) and ApoE (Remaley et al., 2001; Krimbou et al., 2004). Regarding its effect on lipid efflux, the carboxyl-terminal fragment of ApoE (10-kDa-ApoE) induces a strong lipid efflux from non-CNS cells such as macrophages and ABCA1 plays a critical role in this efflux (Vedhachalam et al., 2007). Interestingly, contrary to these findings, 10-kDa-ApoE does not induce lipid efflux from the cultured neurons and astrocytes (Fig. 1). The reason for this discrepancy